Conductive Ternary Nitride as an Alternative Material in the Design of Plasmonic Refractive Index Sensor

by

Anika Rahman Habiba (190021136)
Tasmiah Rahman (190021313)
Sumaiya Tasnim Prapti (190021325)

A Thesis Submitted to the Academic Faculty in Partial Fulfillment of the Requirements for the Degree of

BACHELOR OF SCIENCE IN ELECTRICAL AND ELECTRONIC ENGINEERING

Department of Electrical and Electronic Engineering
Islamic University of Technology (IUT)
Gazipur, Bangladesh
June 2024

Certificate of Approval

Conductive Ternary Nitride as an Alternative Material in the Design of Plasmonic Refractive Index Sensor

Submitted by

Anika Rahman Habiba (190021136)
Tasmiah Rahman (190021313)
Sumaiya Tasnim Prapti (190021325)

has been approved by:

Dr. Rakibul Hasan Sagor

Supervisor and Professor,
Department of Electrical and Electronic Engineering,
Islamic University of Technology (IUT),
Boardbazar, Gazipur-1704.

Date: 25/06/24

Declaration of Authorship

We hereby certify that the thesis titled "Conductive Ternary Nitride as an Alternative Material in the Design of Plasmonic Refractive Index Sensor" represents the outcome of research conducted under the supervision of Dr. Rakibul Hasan Sagor, Professor at the Islamic University of Technology. This work fulfills partial requirements for the degree of Bachelor of Science in Electrical and Electronic Engineering at IUT.

We affirm that this thesis or any part of it, has not been previously submitted for any other degree or diploma. Proper attribution has been given to all consulted sources and published works of others.

Signatures of the Candidates

Anika 25.06.2024

Anika Rahman Habiba
Student ID: 190021136

Tasmiah 25.06.2024

Tasmiah Rahman
Student ID: 190021313

Prapti 25.06.2024

Sumaiya Tasnim Prapti
Student ID: 190021325

Acknowledgement

Firstly, we extend our sincere gratitude to the Almighty Allah for granting us the strength and perseverance to complete this thesis. We deeply appreciate the invaluable guidance and unwavering support of Prof. Dr. Rakibul Hasan Sagor, whose insights and encouragement were instrumental in shaping our research.

We also thank Mr. Md. Omar Faruque, Mr. Sheikh Montasir Mahbub, and Mr. A. K. M. Rakib for their early guidance and teachings which laid a strong foundation for our work. Our heartfelt thanks go to all faculty members of the Electrical and Electronic Engineering Department at IUT for their support and inspiration throughout our academic journey.

Lastly, we are grateful to our families for their unwavering support, understanding and belief in our abilities.

Anika Rahman Habiba
Tasmiah Rahman
Sumaiya Tasnim Prapti

June, 2024

Table of Contents

List of Tables

List of Figures

List of Acronyms

CMOS	Complementary Metal-Oxide-Semiconductor
EDX	Energy Dispersive X-ray Spectroscopy
ENIAC	Electronic Numerical Integrator and Computer
FOM	Figure of Merit
FEM	Finite Element Method
MIM	Metal-Insulator-Metal
MUS	Material Under Sensing
PDE	Partial Differential Equation
RE	Rare Earth
RI	Refractive Index
SBC	Scattering Boundary Conditions
SERS	Surface-Enhanced Raman Scattering
SPP	Surface Plasmon Polariton
SPR	Surface Plasmon Resonance
SR	Sensing Resolution
TCO	Transparent Conducting Oxide

Abstract

Traditional plasmonic materials such as gold and silver have been widely used in Metal-Insulator-Metal (MIM) plasmonic sensors. However, these materials face significant challenges, including high optical losses, chemical reactivity, and compatibility issues with standard fabrication processes. This thesis investigates the use of conductive ternary nitrides, specifically $Ti_xY_{1-x}N$, as a promising alternative for designing plasmonic refractive index sensors. Employing the Finite Element Method (FEM), the study examines the plasmonic properties of $Ti_xY_{1-x}N$, aiming to overcome the drawbacks of conventional materials. The initial parameters of the proposed sensor achieved a sensitivity of 513.3085 nm/RIU. After optimization, the sensor demonstrated enhanced sensitivity of 819 nm/RIU and an improved FOM of 32 RIU^{-1}. The proposed plasmonic refractive index sensor, utilizing $Ti_xY_{1-x}N$, has demonstrated exceptional sensitivity in air pressure sensing applications, enabling precise detection of minute pressure changes. This capability is particularly beneficial for environmental monitoring and industrial applications where accurate air pressure measurements are crucial. The research provides a comprehensive comparison between $Ti_xY_{1-x}N$ and traditional plasmonic materials, underscoring the advantages of $Ti_xY_{1-x}N$, such as lower optical losses, higher chemical stability, and better compatibility with existing manufacturing technologies. The findings of this study pave the way for the development of efficient, high-performing plasmonic devices, advancing the fields of nanophotonics and plasmonic sensor technology.

Chapter 1

Introduction

1.1 Plasmonics

Plasmonics is an interdisciplinary field merging optics and nanotechnology that focuses on manipulating and detecting optical signals at the nanoscale level [1][1]. Through the excitation of plasmons or the collective electron oscillations at the metal-dielectric interface, plasmonics enables precise control over light-matter interactions [2]. This control extends to enhancing light absorption, scattering and confinement within nanoscale regions, surpassing the limitations of conventional optics [3]. Notably, materials like gold, silver and graphene exhibit unique plasmonic properties under investigation by researchers [4].

One significant application of plasmonics lies in enhancing molecular detection sensitivity through techniques like surface-enhanced Raman scattering (SERS) [1][1]. By leveraging the intense electromagnetic fields associated with plasmons, SERS allows for the detection of trace amounts of substances with significant implications for chemical and biological sensing [2]. Additionally, plasmonics facilitates the development of compact and efficient photonic devices, such as plasmonic waveguides, essential for advancing technologies like optical computing and data storage [3]. Through ongoing research into novel materials and advanced fabrication techniques, the efficiency and functionality of plasmonic devices continue to evolve, promising further breakthroughs in nanophotonics [4].

1.2 Surface Plasmon Polaritons

Surface plasmon polaritons (SPPs) are electromagnetic waves that travel along the interface between a metal and an insulator. These waves are formed by the collective motion of electrons on the metal surface interacting with electromagnetic waves on the insulator surface [1]. SPPs became well-known in surface science due to Ritchie's pioneering work in the 1950s [5]. They are attracting significant interest from a broad spectrum of scientists, including physicists, chemists, materials scientists and biologists. Recent technological advances allow for the precise structuring and analysis of metals at the nanometer scale which enables researchers to control SPP properties and uncover new scientific aspects while developing specific applications.

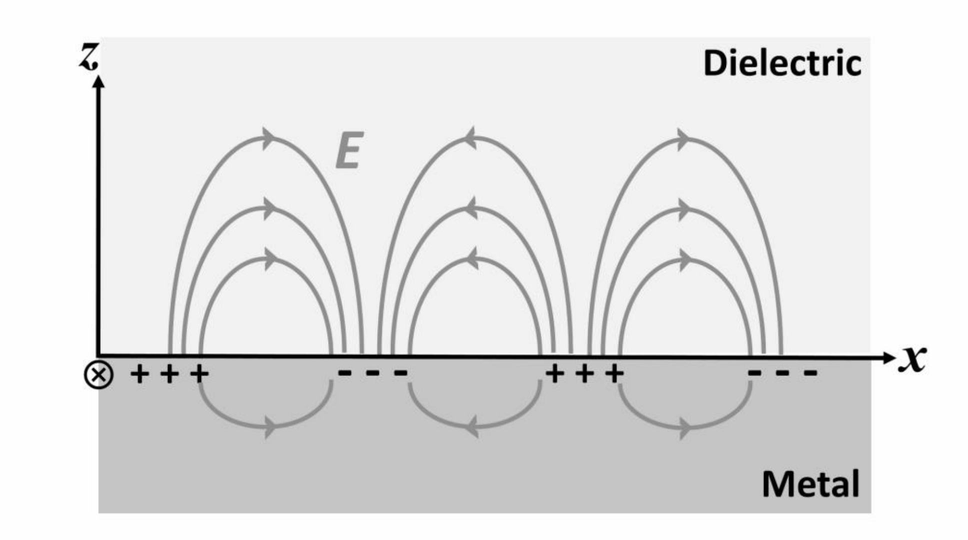

Figure 1. 1: Propagation of SPP along metal-dielectric interface

One remarkable characteristic of SPPs is their ability to surpass the diffraction limit which confines light to subwavelength dimensions [2,3]. This unique property enables the creation of nanoscale plasmonic devices with diverse applications, such as refractive index sensors [4,6-8], filters [9,10], switches [11,12], demultiplexers [13,14], couplers [15], splitters [16,17] etc. For instance, SPP-based refractive index sensors offer high resolution and sensitivity that make them suitable for various applications including biomedical sensing and environmental monitoring [4,6-8]. Similarly, SPP-based filters and switches provide opportunities for controlling light at the nanoscale level incorporating advancements in optical communication and signal processing [9-12]. Moreover, SPP-based demultiplexers, couplers and splitters play crucial roles in photonics by enabling the manipulation and distribution of optical signals in compact and efficient systems [13-17]. These devices hold promise for applications in telecommunications, data processing and integrated photonics.

1.3 Plasmonic Waveguide Topologies

Plasmonic waveguides are nanoscale structures designed to guide and manipulate surface plasmon polaritons (SPPs), exploiting the interaction between light and SPPs for controlled propagation. Unlike traditional dielectric waveguides which rely on total internal reflection, plasmonic waveguides confine light through metal-dielectric interfaces enabling subwavelength confinement and enhanced light-matter interactions [18]. Various waveguide topologies have been developed to harness SPP propagation, each offering unique advantages and applications.

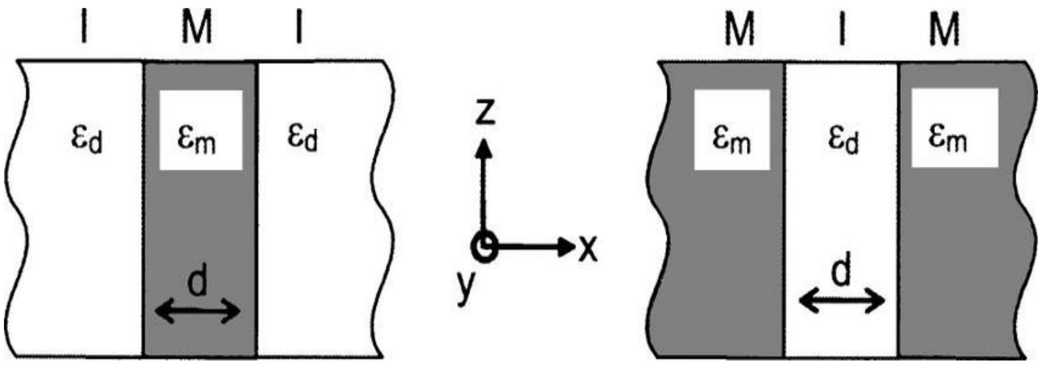

Figure 1. 2: IMI (left) and MIM (right) Waveguide Topologies

The Metal Insulator Metal (MIM) waveguide is a prominent choice in the realm of plasmonic waveguides, particularly in designing refractive index (RI) sensors [19]. This waveguide configuration consists of a dielectric medium sandwiched between two metal layers, facilitating the guidance of surface plasmon polariton (SPP) waves along the metal-dielectric interface [20]. MIM waveguides offer remarkable properties such as strong electromagnetic field confinement, low propagation loss, effective interference and straightforward fabrication, making them highly suitable for nanosensor applications [21, 22]. The confinement ability of the MIM waveguide ensures precise control over the guided wave and its interaction with surrounding materials, which is essential for RI sensing applications [23]. Despite having a relatively shorter propagation length compared to other waveguide topologies, the MIM waveguide exhibits lower propagation loss, indicating minimal attenuation and improved signal quality [24]. This characteristic has garnered significant interest from researchers and industry professionals alike, leading to the widespread utilization of MIM waveguides in the production of efficient and high-performing photonic devices [25]. Additionally, the compactness and efficiency offered by MIM waveguides make them preferred choices for integrated photonics and optical sensing applications [26].

In contrast to the MIM waveguide, the Insulator Metal Insulator (IMI) waveguide presents a distinct arrangement with a metal layer positioned between two layers of dielectric material [27]. The IMI waveguide is capable of supporting long-range Surface Plasmon Polariton (SPP) waves, making it suitable for nanodevices requiring extensive wave coverage [28]. However, the IMI waveguide faces limitations in terms of electromagnetic wave confinement compared to the MIM waveguide [29]. The reduced confinement in the IMI topology compromises the effective interaction between the guided wave and surrounding materials, potentially affecting device sensitivity and efficiency [30]. While the IMI waveguide offers extended propagation length, its limited confinement ability poses challenges in creating highly sensitive structures for RI sensing applications [31].

Despite the advantages of the IMI waveguide in supporting long-range SPP waves, the MIM waveguide remains a preferred choice for RI sensors and other applications requiring strong electromagnetic field confinement [32]. The MIM waveguide offers superior confinement ability, ensuring precise control over light-matter interactions and enabling the development of highly sensitive photonic devices [33]. Additionally, the lower propagation loss of the MIM waveguide enhances signal integrity and transmission efficiency, making it an attractive option for various optical applications [34].

1.4 Plasmonic Refractive Index Sensor

Plasmonic refractive index (RI) sensors are highly regarded within the field of plasmonics due to their compact size and exceptional sensitivity [34]. These sensors operate based on the principle of surface plasmon resonance (SPR), which occurs when light induces collective oscillations of electrons at the interface between a metal and a dielectric. This interaction is highly sensitive to changes in the refractive index of the surrounding medium, making plasmonic RI sensors ideal for detecting various substances.

These sensors have a broad range of applications. They are widely used to detect different dielectric materials, including gases, chemicals, biomolecules, viruses and even cancer cells, with very high sensitivity [35]. The ability of plasmonic RI sensors to detect such a wide array of substances makes them invaluable in medical diagnostics, environmental monitoring and chemical analysis. Researchers are actively working on improving various performance metrics of these sensors, such as sensitivity, resolution, quality factor, and figure of merit [1]. Sensitivity enhancement is particularly crucial, as it determines the sensor's ability to detect minute changes in the refractive index. High-resolution sensors can distinguish between substances with very similar refractive indices, which is important for applications requiring precise detection.

Moreover, advancements in nanofabrication techniques have enabled the development of plasmonic structures with optimized geometries, further enhancing the performance of these sensors [36]. Innovations such as using different materials and composite structures are also being explored to push the boundaries of what plasmonic RI sensors can achieve.

1.5 Thesis Objective

The primary objective of this thesis is to explore and identify a viable alternative to conventional plasmonic metals, aiming to mitigate their inherent limitations. This alternative material should exhibit similar plasmonic properties while overcoming issues such as high optical losses, chemical reactivity and incompatibility with standard fabrication processes. The detailed objectives of the thesis are as follows:

- **Study of Conventional Plasmonic Metals and Their Optical Properties:** Conduct a comprehensive review and analysis of commonly used plasmonic metals such as gold and silver, focusing on their interaction with light, surface plasmon resonance (SPR) characteristics and limitations.
- **Identification of Alternative Materials:** Investigate potential materials that could replace traditional plasmonic metals. The goal is to find materials that exhibit lower optical losses, higher chemical stability and better compatibility with existing manufacturing technologies.
- **Mathematical Modeling:** Develop mathematical models to describe the optical properties and plasmonic behavior of the identified alternative materials using established theoretical frameworks.
- **Theoretical and Experimental Comparison:** Validate the mathematical models by comparing their predictions with experimental data. This step is crucial to ensure that the theoretical models accurately represent the physical behavior of the alternative materials.
- **Design and Optimization of Plasmonic Devices:** Leverage the newly developed waveguides to design advanced plasmonic devices. Optimize these designs to enhance performance metrics such as sensitivity, quality factor, and figure of merit, thereby demonstrating the practical advantages of the alternative materials in real-world applications.

1.6 Thesis Layout

This thesis is organized into seven chapters, each detailing different aspects of the research conducted on alternative materials for plasmonic devices and their applications in on-chip refractive index (RI) sensors.

Chapter 1 provides a foundational understanding of plasmonics, including plasmonic waveguides and various plasmonic devices. It highlights contributions from researchers in the field of plasmonic material technology and outlines the scope and objectives of this thesis.

Chapter 2 offers a comprehensive overview of plasmonic refractive index sensors, discussing their applications in nanotechnology and optical sensing. It covers the operational principles of these sensors and compares different types. Additionally, this chapter addresses the conventional plasmonic materials currently used, their properties, and the challenges associated with them.

Chapter 3 details the research methodologies employed to evaluate the effectiveness and applications of plasmonic refractive index sensors. It describes the research design, data collection methods, and analytical techniques used, ensuring the validity and reliability of the study.

Chapter 4 explores potential alternatives to traditional plasmonic metals. It includes the mathematical modeling of these alternative materials, validation of the models through theoretical and experimental comparison and an analysis of their plasmonic properties relative to conventional metals.

Chapter 5 focuses on the development and analysis of a modified hexagon shaped Metal-Insulator-Metal (MIM) refractive index sensor based on $Ti_xY_{(1-x)}N$. The sensor, designed for on-chip applications, is evaluated for its performance in detecting air pressure. The chapter demonstrates the sensor's effectiveness through sensitivity analysis.

Chapter 6 summarizes the key findings and contributions of the research. It revisits the limitations of silver-based RI sensors and highlights the advantages of the proposed $Ti_xY_{(1-x)}N$ based modified hexagon shaped MIM sensor. The chapter also discusses the potential for future research and the broader implications of the findings in the field of plasmonics and nanotechnology.

The final chapter, **Chapter 7**, showcases the application of Outcome Based Education (OBE) principles in the context of the research conducted. It demonstrates how the outcomes of this study align with the educational objectives and goals set forth, highlighting the practical and educational significance of the research.

Chapter 2

Literature Review

Surface plasmon sensors have been popular study subjects since the late 1980s. Performance and quality of a plasmonic sensor are mostly determined by its sensitivity and Figure of Merit (FOM). A refractive index sensor's sensitivity and FOM demonstrate its ability to identify variations in the index. The scientists want to propose a number of geometric configurations to increase the sensitivity and field of vision of the sensors. Several shaped resonators created recently are compared in Table 1.1 for sensitivity and FOM.

Table 2.1: Comparison of sensitivity and FOM of different shaped resonators

Serial No.	Model Structure	Sensitivity (nm/RIU)	FOM (RIU $^{-1}$)	Ref.
1.	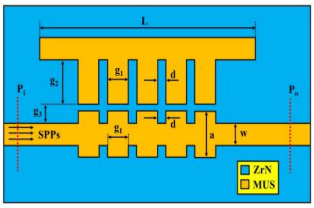	1445.46	140.96	[18]
2.	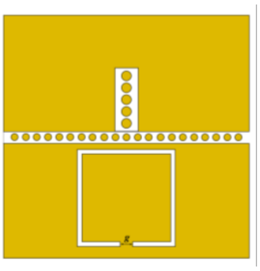	1074.88	32.4	[19]
3	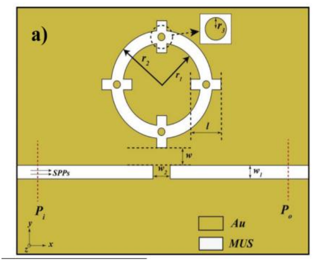	6227.6	6.52	[20]

4	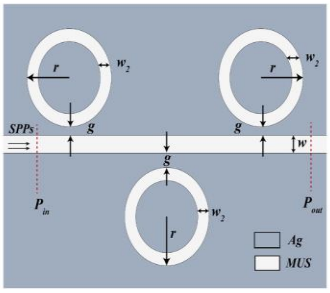	3573.3	21.9	[21]
5	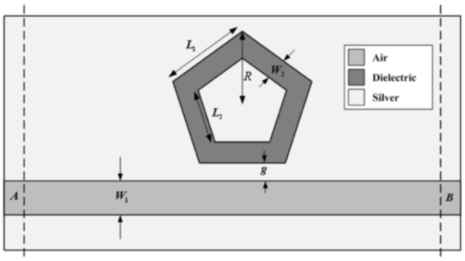	2325	159.6	[22]
6.	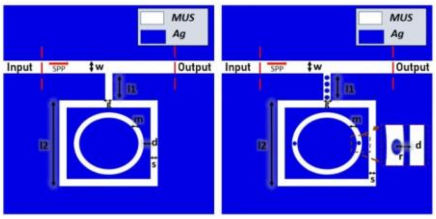	2850	105.95	[23]
7	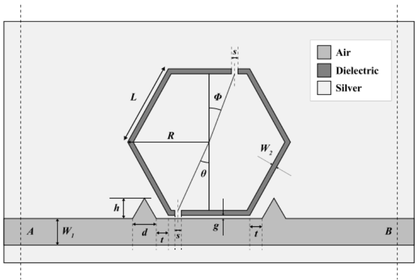	4571.7	63.3	[24]

8	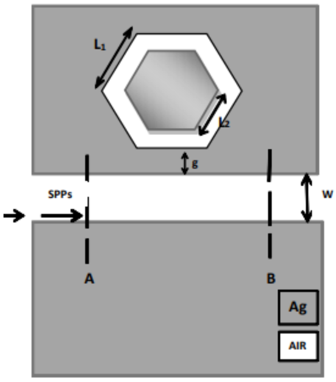	1743	15.6	[25]
9	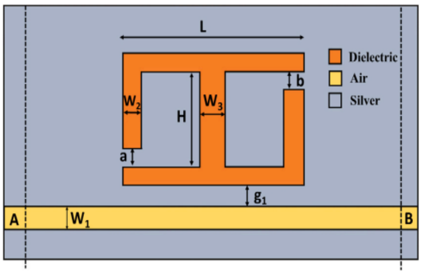	2963.73	25.1	[26]
10	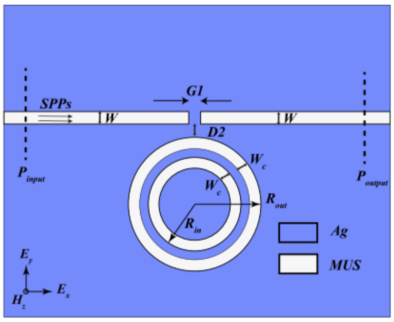	3639.79	91.02	[27]

In the early 40's, there was electrical general-purpose computers which was known as Electronic Numerical Integrator and Computer (ENIAC). At that time, it was used for different computer issues like tuning, reprogramming, etc. Now ENIAC has become gigantic. It weighs 30 tons with 18000 vacuum tubes and 1500 relays [37]. This device has shown many drawbacks like processing speed and computational capacity which is important for modern applications [38].

The maximum bit rate that copper interconnects may transfer between electronic components in a second is constrained. This limit arises from the physics of resistive loss and is scaleinvariant, meaning that it is not greatly affected by expanding or contracting the system [39]. High-speed communication can be achieved by optical interconnects, however integrating fibre optic cables with electronic components in a single circuit has proven challenging due to their 1,000 times bigger size [40]. In this case, surface Plasmon Polaritons (SPPs) are involved. Surface plasmon-based sensors have been the focus of much study since the late 1980s. 1989 saw the introduction by Batchelder et al. of an optical sensor based on SPR that is capable of material detection [41]. Dielectric and metal coatings were integrated with a planar optical waveguide by Lavers et al. (1994) and Harris et al. (1995) to support an SPR-based sensor for an aqueous environment and to detect a change in transmitted power, respectively. More integrated optical surface plasmon resonance (SPR) sensors were demonstrated in the latter part of the 1990s [42–46]. Thin metal films were produced as a substrate for attaching sensor films to integrated optical waveguide systems. These SPR sensors were too big for lab-on-a-chip applications since they were made of dielectric materials with a poor refractive index contrast. Only a small number of additional SPP sensors with different detecting algorithms have been shown. SPP resonance of nanoparticles is one example [47, 48], Further improvement of transmission with nanohole arrays [49, 50]. Vesseur et al. showed in 2008 how to create gold nano-resonators for SPP using focused-ion-6 beam machining [51]. Surface Plasmon Polaritons (SPPs) are being studied in the field of nanoscale electronics as a potential replacement for conventional copper interconnects. There are numerous advantages to using SPPs for this purpose. First off, compared to copper, SPPs may be able to support much larger data densities since their dimensions can be substantially smaller than the wavelength of light. Second, SPPs have the ability to travel at nearly the speed of light, which means they could be able to transmit data more quickly than copper could. Additionally, SPPs are easily connected with current optical systems, including fibre optic cables, which are already in use for long-distance, high-speed data transmission. Lastly, given that devices are becoming smaller and copper wire resistance is increasing, SPPs might be more energy-efficient than copper. However, there are a number of important challenges associated with using SPPs for data transfer. These include loss (because SPPs often disperse over short distances), challenges in producing and identifying SPPs, and the requirement for new materials and manufacturing processes [52]. Silver and gold are both commonly utilized as metals in plasmonic sensors because they can support surface plasmon resonances; nevertheless, each has pros and cons of its own. Compared to gold, silver has a larger imaginary part and a higher negative real part of the dielectric function in the visible spectrum, which can increase the sensitivity and field enhancement of plasmonic sensors. Silver's optical qualities deteriorate with time due to oxidation and sulfation in air. However, gold is more suited for long-term uses or harsh conditions because it is chemically stable and resistant to oxidation and tarnishing. Furthermore, the plasmon resonance of gold is larger, which is beneficial for applications needing a wide spectrum response. Gold is the preferred material for biological and medicinal purposes because it is also biocompatible. Among other uses, gold nanoparticles are widely used in medication delivery, photothermal treatment, and biosensing [53]. Although gold has a larger resonance, is more biocompatible, and is chemically stable than silver, it is nevertheless a more adaptable material for plasmonic sensors, especially in biological and medical applications. The four factors to take into account while creating an "optimal plasmonic sensor," according to Becker, J. et al., are sensitivity, figure of merit, generalized figure of merit, and figure of merit for thin layers [54]. The ratio of the change in the sensor's reaction to a specific alteration in the parameter being monitored is known as sensitivity. This phenomenon is usually utilized in relation to plasmonic sensors and describes how the presence of the target analyte can alter the optical response of the sensor, changing things like light intensity or wavelength in response to changes in the refractive index of the surrounding medium. For applications like illness diagnosis or environmental monitoring, where the analyte may be present in extremely low quantities, high sensitivity is preferred since it makes it possible to detect smaller changes in analyte concentration. A dimensionless metric called Figure of Merit (FOM) is used to evaluate and contrast the performance of various sensors. When referring to plasmonic sensors, the full width at half maximum (FWHM) of the resonance peak in the optical response of the sensor is generally divided by the sensitivity [27]. A smaller FWHM indicates a sharper resonance, which can enhance the sensor's capacity to discern between various analytes or varying concentrations of the same analyte. The full width half maximum (FWHM) is a measurement of the resonance's bandwidth. Consequently, a sensor that performs better is indicated by a larger FOM, which can be attained by having a lower FWHM or a high sensitivity. Essential quality analysis metrics for plasmonic devices utilized in sensing applications are sensitivity and FOM. While a high sensitivity sensor can detect even the smallest changes in analyte concentration, a high FOM sensor can discriminate between distinct analytes or different concentrations of the same analyte with accuracy. A plasmonic resistivity sensor was presented by Y. F. Chou Chau in 2023. It consisted of a metal-insulator metal bus waveguide with a semi-circular ring resonator that was embedded with silver nanorods (AgNDs). Comparing the optical path of the system to a traditional circular resonator, it is shorter. Furthermore, greater coupling is provided by the resonator basement that faces the bus waveguide, increasing the gap plasmon resonance between the incident light and AgNDs. It was found that the gap plasmon mode in the resonator is considerably influenced by the dimension of the AgNDs, which increases the sensitivity of the structure. The device's sensitivity can be increased by 223,07% with the designed structure compared to the standard one. A computed sensitivity of 2900 nm/RIU was the highest [55]. A metal-insulator-metal (MIM) plasmonic sensor with two pairs of coupled bowtie resonators with four silver barriers creating various modes was statistically studied in 2021 by Y. F. Chou Chau. The suggested structure can be used as a plasmonic refractive index and visible and near-infrared glucose sensors. The simulation's findings show that bowtie cavities with silver baffles can change the plasmon resonance modes, offering an adaptable way to increase sensitivity and figure of merit. The highest figure of merit can reach 50.00, 46.67, and 36.00 /RIU, while the maximum sensitivity can reach 1,500.00, 1,400.00, and 1,100.00 nm/RIU throughout modes 1 through 3. With three modes working simultaneously in the visible and near-infrared, the sensor reached a sensitivity of more than 1100 nm/RIU and a FOM not found in previously published research [56]. Yuan-Fong Chou Chau presented a high-sensitivity surface plasmon polariton (SPP)-based sensor in 2020. The sensor has a straightforward design. It was a metal-insulator-metal waveguide with a stub that was defective and had several silver nanorod flaws in it. This sensor is meant to be used with temperature and refractive index sensors. The simulation results show that the sensitivity profile is strongly affected by the presence of silver nanorod flaws in a single segment, offering an additional control parameter over the nanometer-scale system response. By adjusting the stub length, defect rod radius, and number of defects in the stub, the maximum refractive index sensitivity and temperature sensitivity obtained are 5140 nm/RIU and around 2.05 nm/°C1, respectively [57]. In 2021, Rashid et al. presented a refractive index nanosensor with a cog-shaped resonator embedded with gold nanorods with gold as the plasmonic material. Finite Element Method (FEM) was applied in order to examine the sensor's spectrum properties. The simulation's findings demonstrate that the ideal structure has a peak sensitivity of 6,227.6 nm/RIU. Furthermore, the temperature sensitivity of the suggested sensor is tested using five different liquids, with chloroform demonstrating the maximum temperature sensitivity at 6.66 nm/°C. The suggested design can be a suitable substitute for silver-based sensors due to its chemical stability, sufficient performance as a RI sensor, and temperature detecting capabilities [58]. A titanium nitride (TiN)-based RI sensor with a straight waveguide connected to a Square-Ring Resonator (SRR) and a groove was proposed by Tathfif et al. in

2021. To further enhance the sensing capacity, tiny TiN nanoparticles were added to the waveguide and groove. The optimized structure produced a maximum sensitivity of 1074.88 nm/RIU and Figure of Merit (FOM) of 32.4 after the geometric parameters and materials were modified and the properties of the suggested sensor were examined using the Finite Element Method (FEM). TiN offers a number of advantages, such as resistance to oxidation, optical tunability, resilience to high temperatures, and compliance with the conventional Complementary Metal Oxide Semiconductor (CMOS) fabrication process [59]. In 2023, Butt carried out a numerical study on a plasmonic nano-sensor that might detect tuberculosis (TB) in infected blood plasma. The sensor was made up of a metal-insulator-metal (MIM) waveguide. The effective conversion of the dielectric mode into the plasmonic mode is made possible by the use of two Si3N4 mode converters. Although it mostly affects the lungs, tuberculosis (TB) can also damage the kidneys, lymph nodes, and bones. The refractive index of blood plasma infected with tuberculosis is somewhat lower than that of normal blood plasma. This makes the need for a very sensitive sensing device necessary. With a figure of merit of 11.848, the suggested device achieves a sensitivity of about 900 nm/RIU [60]. Dielectric plasmonic sensors should exhibit a noticeable spectrum shift when the refractive index changes or for a specific amount of analyte. Initially, sphere-shaped gold particles [61, 62], Although spherical gold particles were initially employed, gold nanorods soon surpassed them [63] because of their increased sensitivity to refractive index variations [64]. Many approaches have been made to find the ideal plasmonic sensor with this distinctive large spectrum shift for a given change in refractive index, such as rod-shaped gold nanorattles [65], metamaterials [66], employing gold nanorods coated in silver [67], and others.

Chapter 3

Methodology

3.1 Wave Theory

In this section, we look at the theoretical underpinning for our novel alternative material-based refractive sensor design. This sensor uses a metal-insulator-metal structure and surface plasmon resonance (SPR) for sensing. Hence, a good understanding of Maxwell's equations and constitutive relations is necessary. The significance of these equations lies in the description of relation of electromagnetic fields and materials. These equations also play crucial role in electromagnetism and optical physics.

3.1.1 Maxwell's Fundamental Equations

Maxwell's fundamental equations are four equations that describe the behaviour and interaction of electric and magnetic fields. These formulas provide important insights into electromagnetic phenomena by combining the principles of electricity and magnetism. These formulas define the relationship between material properties and electric and magnetic fields, such as magnetic permeability and electric permittivity.

The wave equation, derived from Maxwell's equations, governs the behaviour of electromagnetic waves as they travel through space or various materials. It covers the fundamental concepts that govern the propagation of electromagnetic waves through space and time. Solving the wave equation allows us to foresee and evaluate the properties of electromagnetic waves, such as their direction, speed and power as they travel through various media. Understanding and forecasting the behaviour of electromagnetic waves and their interaction with matter in a range of physical systems and technological applications necessitates the use of Maxwell's equations and the wave equation. Our sensor technology depends on these four equations that articulate the propagation of light and predict electromagnetic waves.

1. **Gauss's Law for Electric Fields:**

   This law establishes a fundamental relationship between electric charges and the electric fields they generate. It is useful to understand how electric fields operate, how charges interact with electric fields, and how charges are distributed throughout systems. It states that,

$$\nabla \cdot D = \rho \tag{3.1}$$

   Here, ρ is the charge density and D is the electric displacement field. Again, the equation $D = \varepsilon E + P$, relates the electric displacement field to the electric field (E) and the polarization of the material (P).

2. **Gauss's Law for Magnetic Fields:**

   According to this law, the total magnetic flux across all closed surfaces is always zero. As a result, there are same number of magnetic field lines entering and exiting the closed surface. The creation of closed loops by magnetic field lines around current-carrying wires or magnetic materials is also suggested. It is expressed as,

$$\nabla \cdot B = 0 \tag{3.2}$$

   Here, $\nabla \cdot B$ represents the divergence of the magnetic field B.

3. **Faraday's Law for Electromagnetic Induction:**

   This equation demonstrates how an electric field is formed in the interaction with a fluctuating magnetic field. The rate of change of the magnetic field is proportional to the induced electric field. The electric fields formed by the time varying magnetic field, produces closed loops. This phenomenon is known as electromagnetic induction. The equation states that,

$$\nabla \times E = -\frac{\partial B}{\partial t} \tag{3.3}$$

   Here, $\nabla \times E$ represents the curl of the electric field E and $\frac{\partial B}{\partial t}$ is the time rate of change of the magnetic field B.

4. **Ampere-Maxwell Law:**

   The total current which encompasses both conduction and displacement currents is directly proportional to the magnetic field's circulation. The law demonstrates that a magnetic field can be generated by a changing electric field, in a manner similar to the way a changing magnetic field induces an electric field, as outlined in Faraday's law. The equation is formulated as,

$$\nabla \times B = \mu_0 J + \mu_0 \epsilon_0 \frac{\partial E}{\partial t} \quad (3.4)$$

Here, J is the current density and μ_0 and ϵ_0 are the permeability and permittivity of free space respectively.

3.1.2 Electromagnetic Wave Equations Derivation

The wave equation describes how electromagnetic (EM) waves propagate across time and space in various mediums, including vacuums. The derivation of the wave equation from Maxwell's equations is as follows:

We consider the condition of a source-free region for the sake of simplicity. Hence, the charge density ρ and current density J are both equal to zero. This simplifies the Ampere-Maxwell Law to,

$$\nabla \times B = \mu_0 \epsilon_0 \frac{\partial E}{\partial t} \quad (3.5)$$

Again, applying curl on both sides of Faraday's law gives,

$$\nabla \times (\nabla \times E) = -\frac{\partial}{\partial t}(\nabla \times B) \quad (3.6)$$

We know, the vector identity, $\nabla \times (\nabla \times E) = \nabla(\nabla \cdot E) - \nabla^2 E$ and $\nabla \cdot E = 0$ in a source-free region. Therefore, we obtain,

$$-\nabla^2 E = -\frac{\partial}{\partial t}(\nabla \times B) \quad (3.7)$$

Substituting Ampere-Maxwell law into this equation, we obtain the wave equation for the electric field E in a source free region.

$$\nabla^2 E = \mu_0 \epsilon_0 \frac{\partial^2 E}{\partial t^2} \quad (3.8)$$

Similarly, by taking the curl of Ampere-Maxwell law and proceeding in the same way, we obtain the wave equation for the magnetic field B in a source free region.

$$\nabla^2 B = \mu_0 \epsilon_0 \frac{\partial^2 B}{\partial t^2} \quad (3.9)$$

These wave equations govern the propagation of electromagnetic waves in free space. The speed of propagation of these waves is denoted by c, which is stated as,

$$c = \frac{1}{\sqrt{(\mu_0 \epsilon_0)}} \tag{3.10}$$

3.1.3 Constitutive Relations

Fundamental to comprehending how the sensor functions are the constitutive equations. These equations establish the connection between the electromagnetic field and the material of our device. Through their connection between the electromagnetic field and the material's reaction to it, these equations offer important insights into how materials respond under different field circumstances.

Three fundamental constitutive relations of electromagnetic are electric polarization (P), electric field (E), and electric displacement field (D). They are defined as follows.

Electrical displacement is essentially defined as the displacement of an electric charge across a conductor in an electric field. It assesses charge per unit area and is also known as electric flux density.

$$D = \epsilon_0 E \tag{3.11}$$

Here, free space permittivity of the material is denoted by ε_0. In an electric field, permittivity quantifies a material's capacity to store electrical energy.

An external electric field causes charges in a dielectric material to separate. Under such conditions, the material is said to be polarised. For homogeneous, isotropic, and linear materials, it is denoted by:

$$P = \chi_e \epsilon_0 E \tag{3.12}$$

Here, electric susceptibility is represented by χ_e.

The electric displacement of materials occurs in the presence of an electric field. It can be defined as:

$$D = \epsilon_0 E + \chi_e \epsilon_0 E \tag{3.13}$$

Hence, we obtain,

$$D = \epsilon_0 \epsilon_r E \tag{3.14}$$

Where one may write the relative electric permittivity of the material as, $1 + \chi_e = \varepsilon_r$

Some other relations include Magnetization (M), Magnetic Field Strength (H) and Magnetic Field (B). They are defined as follows.

Magnetic field strength quantifies the strength of a magnetic field at a specific location in the field. It is defined as:

$$H = \frac{B}{\mu_0} \tag{3.15}$$

Here, the material's free space permeability is denoted by μ_0. A material is said to be permeable if it can carry a magnetic field.

Comparable to electric polarization, we also have the idea of magnetic polarization or magnetization (M) in reaction to a magnetic field. Consequently, the whole connection between H and B including the magnetization component is:

$$B = (H + M)\mu_0 \tag{3.16}$$

Here, μ_0 is the permeability of free space. The following equation characterizes the magnetization of linear, isotropic, homogeneous materials:

$$M = \chi_m H \tag{3.17}$$

Here, the magnetic susceptibility of a substance is denoted by χ_m.

We thus obtain,

$$B = \mu_0 \mu_r H \tag{3.18}$$

Here, relative permeability of the material is given by $\mu_r = 1 + \chi_m$.

Final relations include Current Density (J) and Electric Field (E). Their relations are shown below.

Electric current density is the quantity of electric current flowing per unit cross-sectional area. The current density rises with increasing current through a conductor. It is stated as:

$$J = \sigma E \tag{3.19}$$

Here, the conductivity of a material is denoted by σ. It shows how readily electric current may pass through the material.

3.2 Material Modeling

At larger level of frequencies, high frequency dependent features of materials include relative permittivity (ε_r) and refractive index (n). This frequency reliance has been quantified by the development of several models. These models include the Lorentz Oscillator model, the Drude model and the Lorentz-Drude model. Our sensor functions only when we can comprehend how electrons in a material respond to an applied electric field. Each of these models offers a different viewpoint on this process. It is possible to properly characterize often used plasmonic materials like gold and silver with these models. With the suitable tabular values, their behavior is modelled.

Our research depends critically on material modeling. It gives surface plasmon resonance and metal-light interaction behavior a theoretical foundation for comprehension and prediction. Finite element approach is used by numerical simulation tools such as COMSOL Multiphysics Software. This software is used to approximate the field inside a triangular mesh that discretizes the system boundary. Both incoming and outgoing signals have transparent boundaries simulated by scattering boundary conditions. Important properties of two-port electromagnetic wave-based devices are transmittance and reflectance. These are measured using scattering parameters. Fundamental mode propagation can be predicted via mode analysis and boundary mode analysis, enabling the identification of parameters including the propagation constant and other pertinent details.

3.2.1 Lorentz Oscillator Model

An extensively used model for comprehending the behavior of materials under electromagnetic fields is the Lorentz material model, sometimes referred to as the Lorentzian or Lorentz-Oscillator model. Among other physics disciplines, it is a crucial material model for comprehending the behavior of dielectric materials. It finds many applications in condensed matter physics, optics and electromagnetics. According to the Lorentz model, harmonic oscillators can be used to describe individual or groupings of particles within a material. With intrinsic resonance frequencies, these oscillators interact with the incident electromagnetic field to produce a complicated dielectric response. This model's fundamental idea holds that oscillations in the material's electronic charge distribution around an equilibrium point are caused by an applied electric field.

The Lorentz model, in contrast to the Drude model, holds that electrons are attached to atoms and move about their equilibrium locations. The electrons' equilibrium locations shift when an external electric field is introduced. The displacement is proportional to the restoring force that brings the electron back to equilibrium. The damping force is related to the electron's velocity and serves to make up for energy lost in collisions and other interactions. That system resembles a damper and spring.

It is possible to solve the electron's equation of motion in these circumstances to obtain a material's polarization expression in terms of an external electric field. The electric permittivity of the material is expressed by the sensing technique and it characterizes its reaction to an electric field. An electron has the following equation of motion when there is an external electric field $E(t)$:

$$m\frac{d^2x}{\partial t^2} = -eE(t) - m\gamma\frac{dx}{dt} - m\omega_0^2 x \tag{3.20}$$

Here,

m = mass of the electron

e = charge of the electron

$E(t)$ = applied external electric field

x = displacement of the electron from its equilibrium position

$\omega_0 =$ is the resonant frequency

γ = damping constant

The equation of polarization $P(\omega)$ can be obtained by analysing the equation of motion in light of a harmonic time dependence, $E(t) = E_0 e^{-i\omega t}$. We get:

$$P(\omega) = \frac{ne^2}{m({\omega_0}^2 - \omega^2 - i\gamma\omega)}E(\omega) \tag{3.21}$$

The electric permittivity is then given by:

$$\epsilon(\omega) = 1 - \frac{{\omega_p}^2}{{\omega_0}^2 - \omega^2 - i\gamma\omega} \tag{3.22}$$

Here, the plasma frequency is denoted by ω_p. Upon further analysis of the equation, it can be extended as follows:

$$\epsilon(\omega) = 1 - \sum_{j=1}^{m} \frac{f_j {\omega_p}^2}{{\omega_j}^2 - \omega^2 + i\gamma_j\omega} \tag{3.23}$$

3.2.2 Drude Model

The traditional framework of the Drude-Lorentz model, sometimes referred to as the Drude material model, explains the reactions of metals and semiconductors under electromagnetic fields. Electrical conductivity and optical characteristics of these materials can be simply described by this model.

In order to describe the electrical and thermal specific characteristics of metal, Paul Drude developed the Drude model in 1900. A metal is shown in this model as a gas of free electrons flowing across a positive ion ocean. Electrons are regarded as free since they can go about the metal without being attached to the atoms. Both collisions with positive charged ions and an external electric field regulate the movement of these electrons. It is thought that these crashes are random, instantaneous phenomena and alter the speed of electron movement. The electrons move uniformly in between collisions.

The equation of motion for an electron moving in the presence of an external electric field *E(t)* is comparable to the Lorentz model. However, there is the exception of the absence of a restoring force component. The relation is presented by:

$$m\frac{dv}{dt} = -eE(t) - m\gamma v \tag{3.24}$$

Here,

m = mass of the electron

e = charge of the electron

$E(t)$ = applied external electric field

v = velocity of electron

γ = damping constant

The equation of motion can be solved in light of a harmonic time dependence, $E(t) = E_0 e^{-i\omega t}$. We get:

$$\epsilon(\omega) = 1 - \frac{{\omega_p}^2}{\omega^2 - i\gamma_0\omega} \tag{3.25}$$

3.2.3 Lorentz Drude Model

One popular classical model for illustrating the reactions of metals and conductors to electromagnetic fields is the Drude model. The characteristics of optical and electrical conductivity of these materials are described in detail and clearly. Though it is basic, the Drude model offers a strong basis for comprehending how conductors react to external influences. But the intricate frequency-dependent behaviour of actual materials is beyond its ability to adequately represent.

The Lorentz-Drude model has demonstrated to give good agreement with experimental data for a broad spectrum of materials. It was developed to overcome limitations of the Drude Model. Reproducibility of experimental data on significant optical parameters including absorption spectra and refractive index has been achieved. The remarkable harmony of the Lorentz-Drude model with experimental results shows its importance in comprehending and predicting the behaviour of real materials. The interactions of electrons inside a substance are considered by the Lorentz-Drude model. In particular in metals and conductors, these interactions are essential to understanding how a material reacts to electromagnetic fields. Including electron-electron interactions into the model will help to understand the collective behaviour of electrons and phenomena like plasmon resonances. These are essential for comprehending the optical characteristics of these materials.

According to this model, the electric permittivity is expressed as:

$$\epsilon(\omega) = 1 - \frac{{\omega_p}^2}{\omega^2 - i\gamma_0\omega} + \sum_{j=1}^{m} \frac{f_j {\omega_p}^2}{{\omega_j}^2 - \omega^2 + i\gamma_j\omega} \tag{3.26}$$

Here, the plasma frequency and the oscillator strength are expressed as ω_p and f_i.

3.3 Surface Plasmon Resonance (SPR)

3.3.1 Dispersion Relation

The dispersion relation describes the dependence of a wave's phase velocity on its frequency. It is crucial for understanding the propagation characteristics of surface plasmon polaritons (SPPs).

The dispersion relation for SPPs can be derived from Maxwell’s equations and the boundary conditions at the metal-dielectric interface. Combining these, the relation can be expressed as:

$$D_0 = \frac{k_{zd}}{\epsilon_d} + \frac{k_{zm}}{\epsilon_m} = 0 \tag{3.27}$$

where k_{zd} is the wave vector component perpendicular to the interface in the dielectric, k_{zm} is the wave vector component perpendicular to the interface in the metal, ϵ_d is the relative permittivity of the dielectric, and ϵ_m is the relative permittivity of the metal.

For SPPs to exist, the permittivity of the adjacent materials must have opposite signs. The wave vector components can be described as:

$$\left(\frac{\omega}{c}\right)^2 \epsilon_i = k_x^2 + k_{zi}^2, \quad i = m, d \tag{3.28}$$

or

$$k_{zi} = \sqrt{\left(\frac{\omega}{c}\right)^2 \epsilon_i - k_x^2}, \quad i = m, d \tag{3.29}$$

where k_x is the continuous wave vector component along the interface due to boundary conditions. The dispersion relation is then given by:

$$k_x = \frac{\omega}{c}\sqrt{\frac{\epsilon_m \epsilon_d}{\epsilon_m + \epsilon_d}} \tag{3.30}$$

As the refractive index of the metal changes with the frequency of light and can be negative, if $\mathrm{Re}(\epsilon_m) < \epsilon_d$, the real part of the SPP wave vector can be expressed as:

$$\mathrm{Re}(k_{spp}) = nk_0\sqrt{1 - \left|\frac{\epsilon_d}{\mathrm{Re}(\epsilon_m)}\right|} > nk_0 \tag{3.31}$$

This implies that the resulting wave vector of the SPP is smaller than the incident wave vector, thus circumventing the diffraction limit.

3.3.2 Sensing Mechanism

The sensing mechanism of our sensor leverages the principles of surface plasmon resonance (SPR) and refractive index sensing. The sensor detects changes in the refractive index of the surrounding dielectric medium. This design allows the resonator to trap light and create resonance. As light travels through the waveguide and enters the resonator, it circulates multiple times around the structure, enhancing its interaction with the dielectric medium and creating resonance opportunities at specific light frequencies.

The resonant wavelength of the light within the structure is influenced by the refractive index of the medium. Thus, any change in the refractive index will cause a shift in the resonant wavelength. The effective refractive index of the Metal-Insulator-Metal (MIM) resonator can be calculated using Maxwell’s equations and boundary conditions at the metal-dielectric interface:

$$k_d \epsilon_m \, tanh\left(\frac{k_d d}{2}\right) + \epsilon_d k_m = 0 \tag{3.32}$$

$$k_{d,m} = \sqrt{\beta_{spp}^2 - \epsilon_{d,m} k_0^2} \tag{3.33}$$

$$\eta_{eff} = \frac{\beta_{spp}}{k_0} \tag{3.34}$$

The sensing process starts by illuminating a port of the sensor with a light source. This light interacts with the metal-insulator-metal structure, exciting surface plasmons at the metal-dielectric interface. These surface plasmons generate electromagnetic waves that travel along the waveguide and couple to the ring resonator, causing resonance at specific frequencies. If the refractive index of the medium changes, for example, due to the binding of a target molecule, the resonance condition will change. This change alters the effective path of the wave by modifying the effective refractive index through a change in the dielectric medium's relative permittivity. Consequently, the resonant wavelength of the light circulating in the hexagonal ring resonator shifts. By monitoring this shift, we can detect the presence and concentration of the target molecule.

3.4 Surface Plasmon Polariton (SPP) Formulation

3.4.1 Propagation and Decaying Property

Surface plasmon polaritons (SPPs) are electromagnetic waves that travel along the boundary between a metal and a dielectric. They are formed by the interaction between electromagnetic waves and the collective oscillations of free electrons at this interface. SPPs are crucial because they can confine light at a very small scale, which is useful in fields like nanophotonics, sensing, and surface-enhanced spectroscopy.

To understand the propagation of an electromagnetic wave with a complex dielectric constant, we use the following equation derived from Maxwell's equations:

$$\nabla^2 E(x,t) = \mu\epsilon \frac{\partial^2}{\partial t^2} E(x,t) \tag{3.35}$$

Here, E represents the electric field, ∇^2 is the Laplacian operator, and $\frac{\partial^2}{\partial t^2}$ is the second partial derivative with respect to time.

Replacing μ with μ0μr and ϵ with ϵ0ϵr , we get:

$$\nabla^2 E(x,t) = \mu_0\mu_r\epsilon_0\epsilon_r \frac{\partial^2}{\partial t^2} E(x,t) \tag{3.36}$$

Knowing that:

$$c = \frac{1}{\sqrt{\mu_0\,\epsilon_0}}$$

$$n = \sqrt{\mu_r\,\epsilon_r}$$

We can rewrite the equation as:

$$\nabla^2 E(x,t) = \frac{n^2}{c^2}\frac{\partial^2}{\partial t^2} E(x,t) \tag{3.37}$$

A solution to this wave equation, representing propagation along the x-axis, is:

$$E(x,t) = E_0 e^{\{i(kx - \omega t)\}} \tag{3.38}$$

Where E_0 is the amplitude of the electric field, k is the wave vector, and ω is the angular frequency.

Substituting this solution into the previous equation, we get:

$$\frac{\partial^2 E}{\partial x^2} = -k^2 E \tag{3.39}$$

$$\frac{\partial^2 E}{\partial t^2} = -\omega^2 E \tag{3.40}$$

The dispersion relation for the plane wave is derived as:

$$k2 = \frac{n^2 \omega^2}{c^2} \tag{3.41}$$

or,

$$k = \pm \frac{\omega}{c} n \tag{3.42}$$

Since n can be complex, we express it as n′+in″, leading to:

$$k = \pm \frac{\omega}{c}(n' + in'') \tag{3.43}$$

Substituting back into the electric field expression:

$$E = E_0 e^{i\left(\frac{\omega}{c}(n'+in'')x-\omega t\right)} \tag{3.44}$$

Simplifying:

$$E = E_0 e^{i\frac{\omega}{c}n'x-\frac{\omega}{c}n''x-i\omega t} \tag{3.45}$$

or,

$$E = E_0 e^{i\beta x-i\omega t} e^{-\frac{\omega}{c}n''x} \tag{3.46}$$

The first term $e^{i\beta x-i\omega t}$ represents wave propagation with propagation constant β. The second term $e^{-\frac{\omega}{c}n''x}$ shows the decay of the electric field amplitude, indicating energy loss as the wave travels.

3.4.2 Propagation at Metal-Insulator Interface

The wave vectors in the metal and dielectric are represented as:

For dielectric:

$$K_d = (K_{1x}, 0, -K_{1z}) \tag{3.47}$$

For metal:

$$K_m = (K_{2x}, 0, -K_{2z}) \tag{3.48}$$

For the metal, the relationship between the wave vector components is:

$$K_{2x}^2 + K_{2z}^2 = \frac{n^2\omega^2}{c^2} = \epsilon_m K_0^2 \tag{3.49}$$

Where:

$$K_{2z}^2 = \epsilon_m K_0^2 - K_{2x}^2 \tag{3.50}$$

Since ϵ_m is negative for metals, K_{2z} will be imaginary if K_{2x} is positive, indicating exponential decay within the metal.

3.4.3 Resonant Wavelength for SPPs

Assuming a TM mode wave propagating in the y-axis direction, the magnetic fields in the metal and dielectric are:

For dielectric:

$$H_{1y} = h_1 e^{ik_{1x}x} e^{-k_{1z}z} \tag{3.51}$$

For metal:

$$H_{2y} = h_2 e^{ik_{2x}x} e^{-k_{2z}z} \tag{3.52}$$

The generalized wave vector is:

$$K_{iz} = \sqrt{K_{ix}^2 - \epsilon_i K_0^2} \tag{3.53}$$

For dielectric:

$$K_{1z} = \sqrt{K_{1x}^2 - \epsilon_d K_0^2} \tag{3.54}$$

For metal:

$$K_{2z} = \sqrt{K_{2x}^2 - \epsilon_m K_0^2} \tag{3.55}$$

Since ϵ_d is positive and ϵ_m is negative, SPPs decay faster in metal than in dielectric.

From the Ampere-Maxwell law:

$$\nabla \times H = \mu_0 J + \frac{\partial D}{\partial t} \tag{3.56}$$

With J=0:

$$\nabla \times H = \frac{\partial D}{\partial t} \tag{3.57}$$

Using $D = \epsilon E$ and $E = E_0 e^{i(kx-\omega t)}$, we get:

$$\nabla \times H = -i\omega\epsilon E \tag{3.58}$$

Equating components, we derive:

$$\frac{K_{1z}}{\epsilon_d} = -\frac{K_{2z}}{\epsilon_m} \tag{3.59}$$

At resonance, the wave vector in the x-direction is:

$$K_{1x} = K_{2x} = K_x \tag{3.60}$$

Resulting in:

$$K_{1x}^2 = \left(\frac{\epsilon_m \epsilon_d}{\epsilon_m + \epsilon_d}\right) K_0^2 \tag{3.61}$$

When K→∞ at resonance:

$$\epsilon m + \epsilon d = 0 \tag{3.62}$$

Assuming $\epsilon_d = 1$, we get ϵ_m = -1. The resonance frequency ω is:

$$\omega = \frac{\omega_p}{\sqrt{2}} \tag{3.63}$$

And the resonant wavelength λ is:

$$\lambda = \frac{\lambda_p}{\sqrt{2}} \tag{3.64}$$

3.4.4 Dielectric Loss Function

When a dielectric is exposed to an alternating field, electronic, ionic, and orientational polarizations contribute to a complex dielectric constant:

$$\epsilon_r = \epsilon_r' - j\epsilon_r'' \tag{3.65}$$

Considering a parallel plate capacitor subjected to an alternating field $E_0 \cos(\omega t)$:

$$D(t) = Q(t) \tag{3.66}$$

The current density is:

$$J(t) = \frac{dD(t)}{dt} \tag{3.67}$$

With $E(t)$ as the electric field intensity:

$$D(t) = \epsilon_0 \epsilon_r E_0 e^{j\omega t} \tag{3.68}$$

Substituting the complex dielectric constant:

$$J(t) = \epsilon_0[\omega\epsilon_r'' E_0 \cos(\omega t) - \omega\epsilon_r' E_0 \sin(\omega t)] \tag{3.69}$$

The instantaneous power absorbed is:

$$W(t) = \frac{1}{2\pi}\int_0^{2\pi} J(t)E(t)d(\omega t) \tag{3.70}$$

Simplifying:

$$W(t) = \frac{\omega}{2}\epsilon_0 \epsilon_r'' E_0^2 \tag{3.71}$$

This shows that the energy absorbed by the dielectric is proportional to ϵ'', known as dielectric loss. The loss tangent is:

$$\tan\delta = \frac{\epsilon_r''}{\epsilon_r'} \tag{3.72}$$

This factor measures energy dissipation in the dielectric material.

3.5 Method of Simulation

Most physical processes are temporally and spatially dependent by nature, including wave propagation, fluid dynamics, and thermal analysis. These processes are described mathematically by partial differential equations (PDEs). Nevertheless, analytical solutions for these PDEs are very challenging when dealing with complex geometries and heterogeneous media. By discretization of system boundaries, numerical methods are utilized to approximate solutions, hence solving this challenge. Supporting these numerical approximations thus calls for computer programs.

3.5.1 Finite Element Method

The finite element method is a widely used numerical instrument for the solution of partial differential equations (PDEs). The FEM is renowned for its precision and efficiency, particularly in the context of irregular geometries. The method entails the division of the subject of interest into smaller, related sections, which are referred to as finite elements. By discretizing the domain, the PDEs can be converted into an algebraic equation system that can be resolved using computer methods. Subsequent FEM is capable of accommodating complex geometries and inhomogeneous media due to the local approximation of the unknown functions within each finite element. The FEM is capable of accurately describing the behavior of the physical system under study as a result of these approximations, which are frequently represented by piecewise polynomials. The finite element method (FEM) has numerous advantages over other numerical techniques, including the finite difference method and the method of moments. Initially, the FEM is more appropriate for irregular geometries due to the fact that the finite elements can be adjusted to accommodate the desired geometry. Secondly, the FEM enables the integration of numerous finite element types into a single simulation, thereby accommodating modifications in material properties or geometric qualities. Lastly, the FEM's capacity to adaptively modify the geometry contributes to the reduction of processing costs in less critical components and the enhancement of accuracy in areas of interest.

The finite element method (FEM) typically involves four stages.

3.5.1.1 Discretization of the Solution Domain

The first step in FEM involves discretizing the solution domain into smaller, simpler parts called finite elements. These elements can be one-dimensional (lines), two-dimensional (triangles, quadrilaterals) or three-dimensional (tetrahedrons, hexahedrons). The points where these elements intersect are known as nodes. The process transforms a continuous problem into a discrete one that can be solved numerically. For example, the solution $V(x,y)$ can be approximated as:

$$V(x,y) \approx e = 1 \sum NVe(x,y) \tag{3.73}$$

where $V_e(x, y)$ represents the solution within each finite element e and N is the total number of finite elements.

3.5.1.2 Element Governing Equations

Each finite element within the discretized domain is governed by differential equations that describe the physical behavior of the problem. For example, consider a triangular element with nodes at (x_1, y_1), $(x_2, y_2)$and (x_3, y_3). The potential V_e at any point within the element can be approximated using a linear function:

$$Ve(x, y) = a + bx + cy \tag{3.74}$$

The coefficients a, b and c are determined using the potentials at the nodes:

$$\begin{pmatrix} V_{e1} \\ V_{e2} \\ V_{e3} \end{pmatrix} = \begin{pmatrix} 1 & x_1 & y_1 \\ 1 & x_2 & y_2 \\ 1 & x_3 & y_3 \end{pmatrix} \begin{pmatrix} a \\ b \\ c \end{pmatrix} \tag{3.75}$$

Solving this system yields the coefficients a, b and c, which can then be used to express the potential within the element as:

$$Ve = \sum_{i=1}^{3} 3\alpha i(x, y)Vei \tag{3.76}$$

The shape functions α_i are given by:

$$\alpha_1 = \frac{1}{2A}[(x_2y_3 - x_3y_2) + (y_2 - y_3)x + (x_3 - x_2)y] \tag{3.77}$$

$$\alpha_2 = \frac{1}{2A}[(x_3y_1 - x_1y_3) + (y_3 - y_1)x + (x_1 - x_3)y] \tag{3.78}$$

$$\alpha_3 = \frac{1}{2A}[(x_1y_2 - x_2y_1) + (y_1 - y_2)x + (x_2 - x_1)y] \tag{3.79}$$

Here, A is the area of the triangular element.

3.5.1.3 Assembling of Element Equations

The next step involves assembling the equations from all elements into a global system that represents the entire domain. The energy associated with each element can be expressed as:

$$W_e = \frac{1}{2}\int \epsilon|\nabla V_e|^2 dS \tag{3.80}$$

Using the shape functions, this energy can be written in matrix form:

$$W_e = \frac{1}{2}\epsilon[V_e]^T\left[C^{(e)}\right][V_e] \tag{3.81}$$

Here, $\left[C^{(e)}\right]$ is the element coefficient matrix. For multiple elements, these local matrices are combined into a global coefficient matrix $[C]$, ensuring continuity across element boundaries. The global system of equations then becomes:

$$W = \sum_{e=1}^{N} W_e = \frac{1}{2}\epsilon[V]^T[C][V] \tag{3.82}$$

3.5.1.4 Solving the System Equations

The final step involves solving the global system of algebraic equations. For Laplace's equation, the condition for minimum total energy leads to:

$$\frac{\partial W}{\partial V_k} = 0$$

which results in a system of linear equations:

$$\sum_{i=1}^{n} V_i C_{ik} = 0 \tag{3.83}$$

Here, n is the number of nodes. This system can be solved using various numerical methods, such as Gaussian elimination or iterative methods like the conjugate gradient method.

3.5.2 Scattering Analysis

Scattering analysis in the context of the Finite Element Method (FEM) involves studying how waves interact with objects and boundaries within a given domain. This is particularly important in electromagnetics, where understanding how electromagnetic waves scatter off objects can provide insights into their properties and behaviors.

The vector wave equation for the scattered field E_{sc} is given by:

$$\nabla \times \left(\frac{1}{\mu}\nabla \times E_{sc}(r,t)\right) + \epsilon\frac{\partial^2 E_{sc}(r,t)}{\partial t^2} + \sigma\frac{\partial E_{sc}(r,t)}{\partial t} = -\frac{\partial J_{eq}(r,t)}{\partial t} \tag{3.84}$$

Here, μ is the permeability, ϵ is the permittivity, σ is the conductivity and J_{eq} is the equivalent source current. The equivalent source current is derived from the incident field E_{inc} as follows:

$$\frac{\partial J_{eq}(r,t)}{\partial t} = \nabla \times \left(\frac{1}{\mu}\nabla \times E_{inc}(r,t)\right) + \epsilon \frac{\partial^2 E_{inc}(r,t)}{\partial t^2} + \sigma \frac{\partial E_{inc}(r,t)}{\partial t}\partial t \tag{3.85}$$

The scattered field E_{sc} can then be used to determine how the wave interacts with the object, providing crucial information for applications like radar and antenna design.

3.5.3 Scattering Parameters

Scattering parameters (S-parameters) are used to describe how an electromagnetic wave propagates through and interacts with a multi-port network. S-parameters are especially useful at high frequencies where voltage and current are less well-defined. They provide a way to characterize the reflection and transmission properties of the network.

The general form of the S-parameter equations is:

$$E_{ec} = E_i + \sum_{j=1}^{N} S_{ji} E_j \tag{3.86}$$

Here, E_{ec} is the total electric field at a port,E_i is the incident electric field and S_{ji} are the scattering parameters. For ports without excitation, the equation simplifies to:

scattering parameters. For ports without excitation, the equation simplifies to:

$$E_{ec} = \sum_{j=1}^{N} S_{ji} E_j \tag{3.87}$$

Specific S-parameters for a two-port device are defined as:

$$S_{11} = \frac{\int_{\text{port 1}} (E_{ec} - E_1) \cdot E_1 \, dA_1}{\int_{\text{port 1}} E_1 \cdot E_1^* \, dA_1} \tag{3.88}$$

$$S_{21} = \frac{\int_{\text{port 2}} (E_{ec} - E_2) \cdot E_2 \, dA_2}{\int_{\text{port 2}} E_2 \cdot E_2^* \, dA_2} \tag{3.89}$$

These parameters can be extended to an N-port device, resulting in an $N \times N$ matrix that encapsulates the scattering behavior of the device:

$$S = \begin{pmatrix} S_{11} & S_{12} & \cdots & S_{1N} \\ S_{21} & S_{22} & \cdots & S_{2N} \\ \vdots & \vdots & \ddots & \vdots \\ S_{N1} & S_{N2} & \cdots & S_{NN} \end{pmatrix} \tag{3.90}$$

3.5.4 Miscellaneous Terms

Port Analysis

Ports are critical components in FEM simulations for defining where inputs and outputs occur. The power flow at these ports is often calculated using the Poynting vector, which represents the directional energy flux (the rate of energy transfer per unit area) of an electromagnetic field:

$$S_{avg} = \frac{1}{2}\mathrm{R}(E \times H^{*}) \tag{3.91}$$

Mode Analysis

Mode analysis involves determining the fundamental modes that can propagate through waveguides or other structures within the simulation domain. The propagation constant k is a complex number that describes both the phase change per unit length and the attenuation due to losses:

$$k = k' + jk'' \tag{3.92}$$

Here, k' is the real part representing the phase constant, and k'' is the imaginary part representing the attenuation constant. This analysis helps in understanding how different modes propagate and attenuate within the medium.

Boundary Conditions

Properly defining boundary conditions is crucial for accurate FEM simulations. Boundary conditions ensure that the simulated fields behave realistically at the edges of the domain. Common types include:

1. **Scattering Boundary Conditions**: Used to simulate open boundaries where waves can exit the simulation domain without reflecting back.

$$E = E_s e^{-jk(n \cdot r)} + E_0 e^{-jk(K \cdot r)} \tag{3.93}$$

   Here, E_{sc} is the scattered field, $E_0$is the incident plane wave, k is the wave number and$n$ is the unit normal vector to the boundary.

2. **Port Boundary Conditions**: Define the locations where waves enter or exit the simulation domain, ensuring accurate modeling of input and output interactions.

By incorporating these detailed analyses and terms, the Finite Element Method can provide comprehensive and accurate solutions to complex physical problems across various domains, including electromagnetics, structural analysis, and fluid dynamics.

3.6 Parameters for Performance Evaluation

3.6.1 Reflectance

Reflectance of a surface or optical instrument control how much light is reflected off of it. When light is focused onto a surface it is equivalent to the incident to reflected power ratio. Integrating each reflected signal into a surface yields the reflectance measurement. The total reflected power of the incident beam is used to normalise the reflecting surface that is formed by integrating the reflected light from the sample. Reflectance is expressed by the equation [109]:

$$|S11|^2 \tag{3.94}$$

or,

$$20log_{10}|S11|dB \tag{3.95}$$

3.6.2 Sensitivity

The way an output of a sensor changes in reaction to an input is known as its sensitivity (S). In the sensor's case, it is the concentration of the analyte. With reference to our refractive index sensor, it is defined as the change in resonant wavelength as ascertained by the interrogation technique per unit change in refractive index.

When $\Delta\eta$ denotes the change in refractive index and $\Delta\lambda$ the wavelength shift, sensitivity is defined as:

$$S = \frac{\Delta\lambda}{\Delta\eta} \tag{3.96}$$

More sensitivity enables the identification of more exact and minute variations in the concentration of the analyte. The sensor sensitivity is established through COMSOL Multiphysics modelling. It is done through changing the refractive index and seeing how the output of the sensor varies concurrently is physics.

3.6.3 Figure of Merit

The Figure of Merit (FOM) is an evaluation of the resolution and sensitivity of the sensor taken together. The traditional method of detecting FOM in case of plasmonic sensors is given by the following equation:

$$FOM = \frac{S}{FWHM} \tag{3.97}$$

Here, $FWHM$ is the full width at half maximum of the resonance dip and S is sensitivity. A better performance is indicated by a higher FOM. Overall sensor performance is measured by the FOM. Like sensitivity, the FOM is as well empirically determined. The computation of FWHM uses the average of the maximum and minimum transmittance around the place of interest. Subtracting the two wavelengths that cross the average transmittance line yields the FWHM.

3.6.4 Quality Factor

A resonator's quality factor (Q) tells how sharp the peak or valley of the resonant dip is. Increased quality factors point to better resolution for identifying changes in the refractive index. It is applied to performance evaluation of filters. It is defined as:

$$Q = \frac{\lambda_{resonant}}{FWHM} \tag{3.98}$$

3.6.5 Sensing Resolution

Sensing resolution (SR) of a refractive index sensor is the smallest change in refractive index that it is identified or resolved. It is a significant indication of the sensor’s functions and sensitivity to variations in the refractive index of the medium indicator. A sensor with a lower sensing resolution can detect bigger refractive index changes. However, a sensor with a higher sensing resolution may detect changes in minute details. It is mathematically expressed as:

$$SR = \frac{\Delta\lambda}{S} \tag{3.99}$$

Chapter 4

Exploring Alternative Plasmonic Materials Beyond Conventional Choices

4.1 Plasmonic Properties of Conventional Materials

Material technology is crucial in advancing plasmonics and plasmonic devices. SPPs are fundamental to these devices, arising from the unique plasmonic properties of materials when illuminated by light. These properties heavily influence the propagation and behavior of SPPs. Plasmonic materials serve as the foundational elements in realizing practical plasmonic devices. Therefore, selecting an appropriate plasmonic material is paramount for achieving high-performance plasmonic devices.

Since plasmonic materials are primarily utilized for their interaction with light, their properties are typically characterized by two parameters: dielectric permittivity, ϵ and magnetic permeability, μ. However, at optical frequencies, the magnetic permeability approaches unity, making the dielectric permittivity the dominant parameter for describing their behavior [68].

The dielectric permittivity of metals is a complex parameter consisting of a real part (ϵ_1) and an imaginary part (ϵ_2). The real part reflects the material's polarization response, while the imaginary part corresponds to optical loss. At optical frequencies, the real part of the dielectric permittivity for metals is negative, a crucial property that enables the generation and propagation of Surface Plasmon Polaritons (SPPs) when illuminated by light. This negative real part of the permittivity is essential for the functionality of plasmonic devices, supporting efficient SPP generation and propagation at material interfaces [69].

Rakic et al. [70] extensively researched the optical properties of metallic films, establishing modelling parameters for eleven metals, prominently including silver and gold. Barchiesi et al. [71] provided optical constants for metals such as gold, silver, aluminium, chromium and titanium, employing the Drude model and Lorentz-Drude model, which are widely used in material modelling.

4.2 Problems with Conventional Plasmonic Materials

Noble metals like Ag (silver) and Au (gold) have been widely used in subwavelength devices due to their sharp resonance, high conductivity, and large free carrier concentrations. Despite these advantages, several limitations hinder the widespread adaptation of these noble metals in plasmonic applications:

1. **Tarnishing Properties**: Silver, a commonly used noble metal, tarnishes when exposed to air or moisture [72,73], forming a layer of silver sulfide [74,75] that significantly degrades its optical properties. The tarnishing process involves the random nucleation of silver sulfide, leading to high-density clusters that deteriorate the performance of plasmonic devices. Gold, while more resistant to tarnishing than silver, is not immune to surface degradation, which can affect its long-term stability and performance in plasmonic applications.
2. **Nanofabrication Challenges**: In plasmonic devices, metals are typically used as thin films. The morphology of metal films differs significantly from bulk metals, which typically have larger grains compared to the smaller grains in thin films. This difference leads to increased grain-boundary scattering losses [76,77], resulting in optical losses that can be three to four times greater than those in bulk metals. Additionally, surface roughness in ultrathin metal films further increases optical loss [78,79]. Special technologies like wetting layers [80] can help mitigate these issues, but they pose limitations in terms of integration and scalability.
3. **Lack of Tunability**: Gold and silver are natural metals with a fixed carrier concentration in the range of 10^{23} cm^{-3}. This high carrier concentration results in a large real and imaginary part of the complex dielectric permittivity, causing problems in plasmonic devices that require a balanced polarization response [81]. Since the carrier concentration cannot be adjusted in natural metals, their dielectric permittivity remains fixed, limiting their use in applications requiring tunable optical properties.
4. **Low Thermal Stability**: Noble metals have relatively low melting temperatures, which results in low thermal stability at higher temperatures [82]. This is particularly

problematic for nanostructures with high surface-to-volume ratios, as they may liquify below their bulk melting points.

5. **Optical Losses**: One of the main disadvantages of conventional plasmonic materials is substantial optical loss due to the large imaginary part of the complex dielectric permittivity. At optical frequencies, loss mechanisms such as interband transitions, intraband transitions, and scattering losses are of considerable significance [83]. These mechanisms increase the imaginary part of the dielectric permittivity, leading to significant optical loss in plasmonic devices formed by metals like silver and gold .
6. **Incompatible Manufacturing Processes:** Noble metals like gold and silver are not compatible with standard silicon manufacturing processes, posing significant challenges for their integration into nanoelectronic components. The diffusion of these metals into silicon forms deep traps that negatively affect device performance [84,85]. This incompatibility hinders the incorporation of plasmonic devices into conventional nanofabrication technologies and nanoelectronics integrated circuits.

In light of these limitations, there is a pressing need to explore alternative materials that can overcome the inherent drawbacks of noble metals and pave the way for the widespread adoption of plasmonic technologies.

4.3 Potential Alternative Materials

Researchers are exploring alternative materials to overcome the limitations of conventional plasmonic metals such as gold and silver while maintaining the ability to produce and propagate Surface Plasmon Polaritons (SPPs). A critical plasmonic property sought after is the negative real part of the complex dielectric permittivity. Various techniques involve modifying material compositions to achieve this behavior, including:

- Heavily doped semiconductors like Ge [86] and Si [87,88] and heavily doped group III-V semiconductors like GaAs, GaN, InP [90],
- Transparent conducting oxides (TCOs) such as heavily doped ZnO, indium oxide, indium tin oxide, cadmium oxide [91,92],
- Other oxides and sulfides like $CdSb_2O_6$, $GaInO_3$, $MgIn_2O_4$ [93],
- Silicides and Germanides [94],
- Interstitial Metal NItrides like titanium nitride, zirconium nitride, tantalum nitride and hafnium nitride [95,96],

- 2D plasmonic materials such as graphene [97],
- Ternary metal nitride systems such as $Ti_xAl_{1-x}N$, $Ti_xY_{1-x}N$ [98].

The primary focus of this thesis is to mathematically model and analyze the plasmonic properties of the last group of materials mentioned above, exploring the blending of a transition metal nitride with other elements such as yttrium.

4.4 $Ti_xY_{1-x}N$ (x = 0.91) as an Alternative Plasmonic Material

TixY1-xN represents a novel class of ternary transition metal nitrides with promising applications in plasmonics, particularly in the infrared spectral range critical for telecommunications. This material is formed by alloying titanium (Ti) with yttrium (Y) in varying compositions (x), which allows for precise tuning of its optical and electronic properties.

4.4.1 Formation of $Ti_xY_{1-x}N$ (x = 0.91)

Opaque polycrystalline $Ti_xY_{1-x}N$ films with thicknesses exceeding 300 nm were deposited under room temperature conditions onto polished stainless-steel substrates using a hybrid reactive arc evaporation−magnetron sputtering process. In this method, titanium vapors were generated via a cathodic arc source, while yttrium was sputtered from a magnetron cathode. The deposition occurred in a reactive atmosphere composed of argon and nitrogen gases at specific flow rates to ensure purity. A substrate bias voltage of −100 V was applied during deposition, and the arc current to the titanium target was maintained at 90 A. The composition of the films, denoted by x, was controlled by adjusting the pulsed DC current applied to the sputtering target using an Advanced Energy Pinnacle + generator operating at 50 kHz frequency with a 4 μs off time. Detailed experimental procedures are documented in reference [98].

To analyze the composition x and the $[N]/[Metal + RE]$ ratios, as well as to determine the crystal structure, various characterization techniques were employed. Sc and Y are the rare earth (RE) materials. Energy dispersive X-ray spectroscopy (EDX) was conducted using a JEOL 840A scanning electron microscope equipped with an Oxford Instruments X-ray analyzer. X-ray diffraction (XRD) measurements were performed in θ-2θ mode using a Bruker (Siemens) D500 apparatus with Co radiation (λ = 0.179 nm) specifically for Ti-based polycrystalline films.

The optical properties of the films were evaluated through spectroscopic ellipsometry to determine the complex dielectric function spectra ($\varepsilon = \varepsilon_1 + i\varepsilon_2$). This analysis covered the spectral range of 0.6−6.5 eV (corresponding to 2067−191 nm) at a 70° angle of incidence. Calibration of spectral intensity distributions was achieved using reflection spectra from an undoped single-crystal Si(001) wafer.

4.4.2 Plasmonic Properties of $Ti_xY_{1-x}N$ (x = 0.91)

Ti/Zr and Sc/Y belong to different groups in the periodic table: Ti and Zr are in group IVb, characterized by four valence electrons in their d orbitals, while Sc and Y are in group IIIb, with three valence electrons in their s orbitals. These elemental configurations influence the properties of their respective nitrides: Ti/Zr nitrides typically exhibit metallic conductivity due to the excess d electrons of the metal, whereas Sc/Y nitrides tend to be semiconducting in nature [99-103].

Both Ti/Zr and Sc/Y nitrides form stable cubic rocksalt (B1) phases when bonded with nitrogen atoms (which have a valence electron configuration of $2s^2\ 2p^3$). This stability allows for the formation of coherent crystalline structures across a range of compositions. Specifically, the ternary $Ti_xSc_{1-x}N$ system maintains stability throughout its entire compositional spectrum in the B1 structure, as supported by various studies [104-106]. In contrast, systems like $Ti_xAl_{1-x}N$ can only stabilize in the B1 phase within limited compositional ranges [103].

The similarities in electron configurations between $Ti_xSc_{1-x}N$ and $Ti_xY_{1-x}N$ suggest that $Ti_xY_{1-x}N$ will exhibit comparable properties to $Ti_xSc_{1-x}N$. Specifically, $Ti_xY_{1-x}N$ is expected to maintain stable B1 phase structures over its compositional range, providing consistency in its material properties.

1. Stable B1 Phase: Similar to $Ti_xSc_{1-x}N$, $Ti_xY_{1-x}N$ is expected to maintain stability in the B1 phase across its compositional range. This phase stability ensures consistent material properties and structural integrity [104-106].

2. Semiconducting Properties: Due to the valence electron configuration of Y, $Ti_xY_{1-x}N$ is expected to exhibit semiconducting behavior. This property is advantageous for applications requiring tunable electrical properties, such as in electronic devices and sensors [99-103].

3. Potential for Infrared Plasmonic Properties: $Ti_xY_{1-x}N$'s electronic configuration and material stability suggest it may extend its plasmonic properties into the infrared range. This capability is crucial for applications in telecommunications and photonics, where infrared wavelengths are commonly utilized [104-106].

4. Negative Real Permittivity: Similar to metals, $Ti_xY_{1-x}N$ exhibits negative real permittivity. This characteristic is crucial for its plasmonic properties, enabling the manipulation of light at infrared wavelengths. It allows for enhanced light-matter interactions, which are beneficial for applications in telecommunications, photonics, and sensing [98].

5. High Electron Conductivity and Mobility: $Ti_xY_{1-x}N$ possesses high electron conductivity and mobility, attributes that stem from its metallic-like nature. These properties are advantageous for applications requiring efficient electron transport, such as in high-speed electronics, microelectronics, and energy harvesting devices.

6. High Melting Point: The material has a high melting point, ensuring stability and durability under high-temperature conditions. This characteristic is essential for applications in harsh environments and processes that involve elevated temperatures, such as in semiconductor fabrication and aerospace components [98].

7. CMOS Compatibility: $Ti_xY_{1-x}N$ is compatible with CMOS (Complementary Metal-Oxide-Semiconductor) processes, a standard technology in semiconductor manufacturing. This compatibility facilitates integration with existing silicon-based electronics and enables the development of novel devices that combine plasmonic functionalities with conventional electronic components.

4.4.3 Comparison with Other Popular Alternative Material

The successful support of Surface Plasmon Polaritons (SPPs) at the interface between $Ti_xY_{1-x}N$ and MUS (metal-dielectric-metal) requires that the permittivity of $Ti_xY_{1-x}N$ exhibits a negative real part, while MUS, being a dielectric material, has a real and positive permittivity. This condition ensures that the electric field normal to the interface changes sign across the $Ti_xY_{1-x}N$-MUS interface, facilitating the propagation of SPPs. Figure 4.1 and figure 4.2 illustrate the real and imaginary parts of the permittivities respectively, demonstrating that $Ti_xY_{1-x}N$ can indeed support SPPs at its interface with MUS. Using the Drude model equation and with the help of the parameter obtained from the supporting information, Real and imaginary parts of permittivity of $Ti_xY_{1-x}N$ in the visible and near-IR spectrum have been plotted using MATLAB software. The parameter values are tabulated in Table 4.1 for composition x of 0.91. For the other values of composition x, the Q_{spp} is lower in the shown optical range in Figure 4.3.

Table 4.1: Drude parameters of $Ti_xY_{1-x}N$ opaque film

x	E_{pu} (eV)	γ_D (eV)
0.91	6.13	0.57

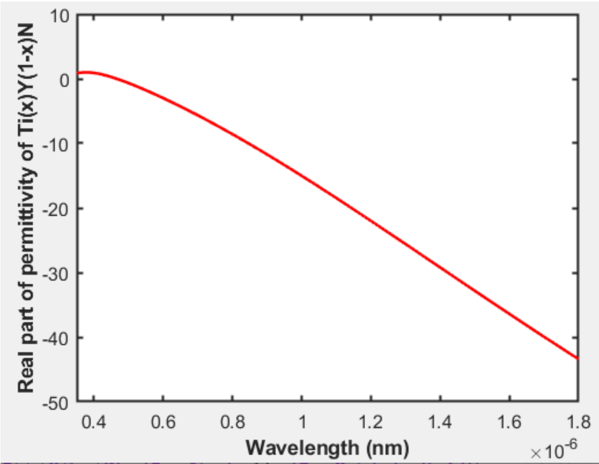

Figure 4.1: Real part of permittivity of $Ti_xY_{1-x}N$ in the visible and near-IR spectrum

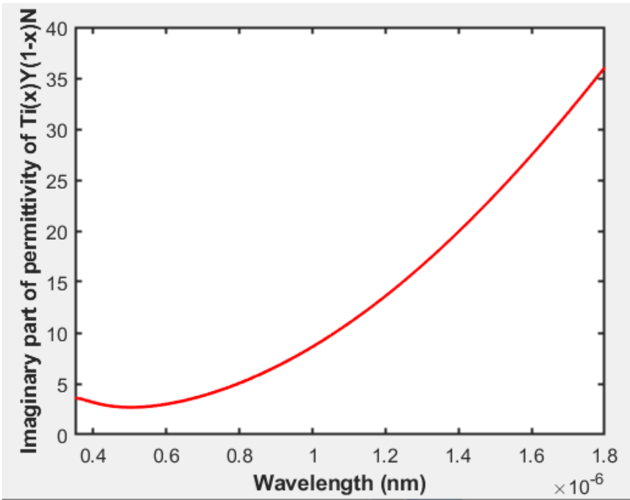

Figure 4.2: Imaginary part of permittivity of $Ti_xY_{1-x}N$ in the visible and near-IR spectrum

Using equation (3.98), comparative analysis of the Quality Factor of SPPs (QSPP) between $Ti_xY_{1-x}N$ and a promising transitional nitride, TiN [107] reveals that $Ti_xY_{1-x}N$ surpasses TiN in supporting high-quality SPPs, especially in the visible spectrum. This superior performance of

$Ti_xY_{1-x}N$ makes it a more suitable choice over TiN for applications requiring efficient SPP support in the visible range. Therefore, the selection of $Ti_xY_{1-x}N$ as a ternary metal nitride shows promise for enhancing the performance of SPP-based sensors and devices.

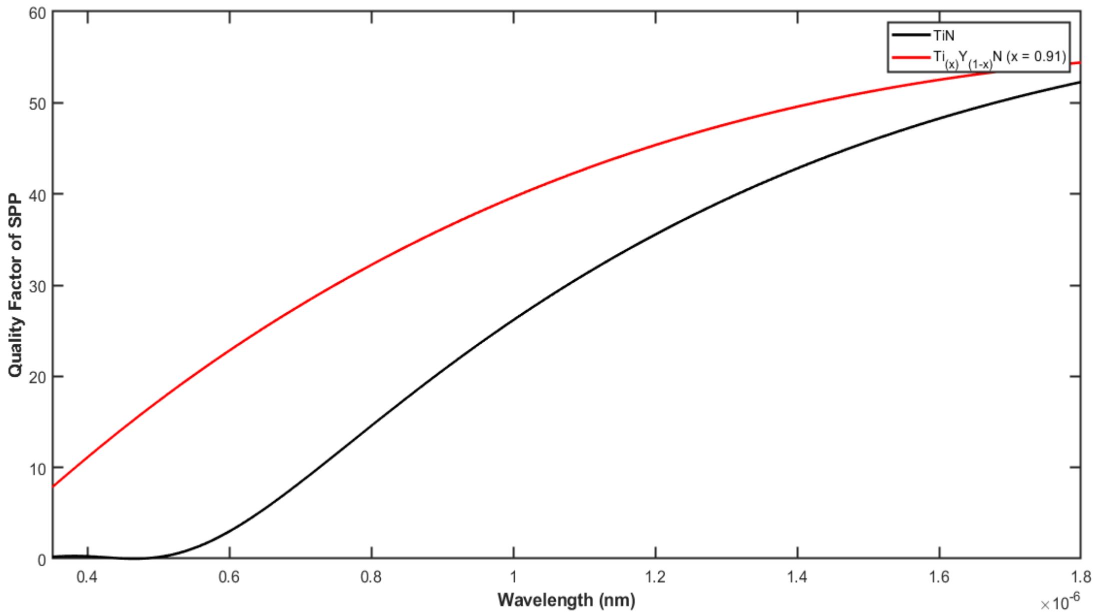

Figure 4.3: Quality Factor of SPP between TiN (Deposited at 500° C) and $Ti_xY_{1-x}N$

Chapter 5

Plasmonic Sensor Design and Performance Analysis

Refractive index sensors need to have their structural properties properly planned and tuned in order to enhance their performance criteria. Significant progress is desired by scientists and engineers in the relationship between light and matter into these sensors by careful choice of parameters and arrangement design, especially with the addition of nanorods, stubs, and baffles. The focus of the many applications made possible by recent developments in refractive index sensors is on measuring different physical quantities and detecting chemical and biological components. While sensor design is essential to best performance, manufacturing process tolerances also need to be taken into account. Thus, it is essential to optimize sensor performance while respecting the tolerance limit for the geometric parameters of the sensor set by the fabrication technology. Size, orientation, and overall structure of the sensors are among the geometric criteria. Additionally influencing a sensor's performance are the materials utilized in its construction. By carefully evaluating and enhancing a sensor's geometric characteristics, researchers can increase its sensitivity and detecting capabilities.

5.1 Basic Structure of Proposed Sensor

The two-dimensional schematic of the proposed plasmonic sensor is comprised of input and output MIM waveguides which anchor-shaped resonator. The MIM waveguide's input port is located on the left, and its output port is located on the right. In figure 5.3, the yellow shaded area represents the silver ($Ti_xY_{x-1}N$) and, the grey shaded zone represents the material under sensing (MUS). The used material Titanium yttrium nitrate is an alternative material that performs better in terms of sensitivity and detectability than other alternative materials like TiN. Table 5.1 presents the basic structural parameters of the proposed refractive index (RI) nanosensor. The distance between the extended part of the resonator and the waveguide is denoted by G and has a value of 15 nm. Also, the distance between the middle part of the resonator and the waveguide is denoted by g which is 11 nm. The radius of the outer circumcircle of the resonator is 250 nm, and the inner circumcircle value is 180nm. The width of the waveguide is denoted as W1 and is 90 nm wide. The resonance has a width denoted by W2, which also measures 70 nm. Initially, the structure with these values.

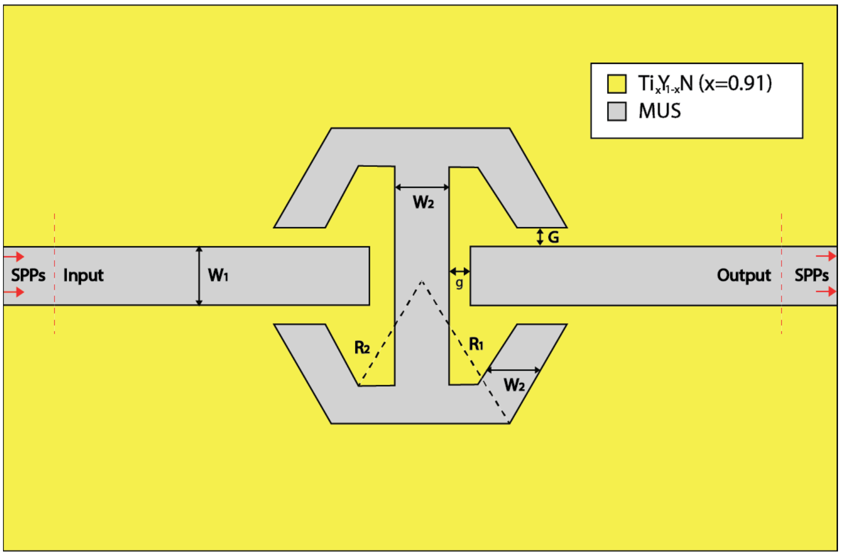

Figure 5. 3: Two-dimensional (2D) schematic of the proposed RI sensor

Table 5.1: Initial Parameters of Proposed Structure

Parameters	Symbols	Values (nm)
Width of Waveguide	W1	90
Width of Resonator	W2	70
Gap between extended part of resonator and waveguide	G	15
Gap between middle part of resonator and waveguide	g	11
Radius of Resonator's outer circumcircle	R1	250
Radius of Resonator's inner circumcircle	R2	180

5.2 Initial Results Obtained

All computations for the proposed work are done in MATLAB and the finite element technique (FEM) is used in COMSOL Multiphysics. The physical interface is the electromagnetic wave frequency domain (ewfd) for short. While absorbing illusive EM-field energies, scattering boundary conditions (SBC) permit restricted reflection. We employ a triangle mesh with very fine features for discretization.

The resonant wavelength is that at which the transmittance peaks appear. When the refractive index or perceived dimensions of the RI sensor change, the resonant wavelengths move to a longer or shorter wavelength region, identifying an unknown material. An RI sensor needs to follow this approach.

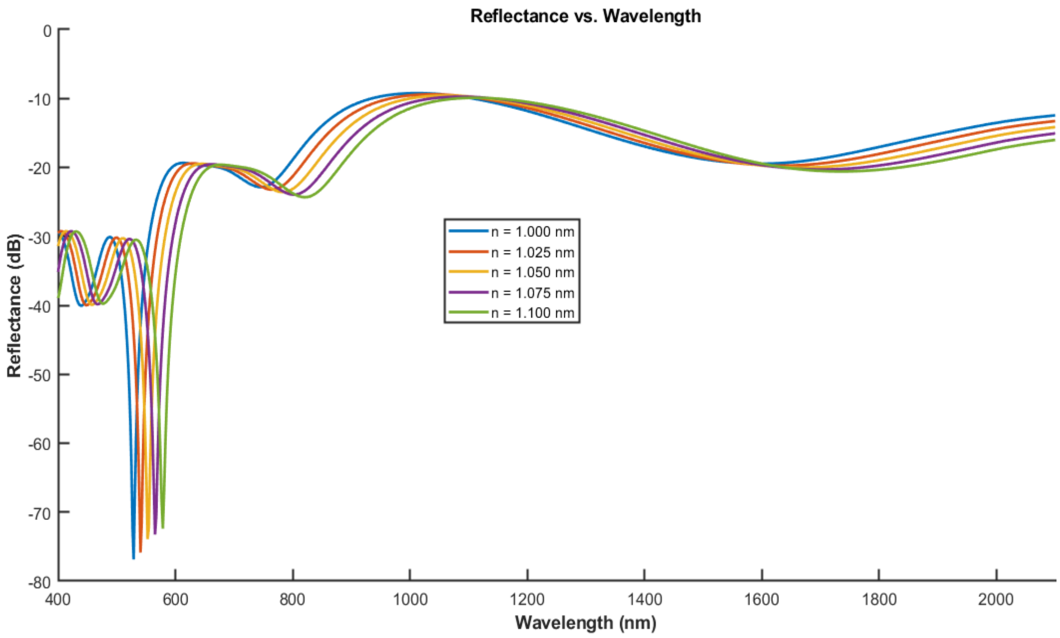

Figure 5. 2: Reflectance vs Wavelength Graph of Initial Results

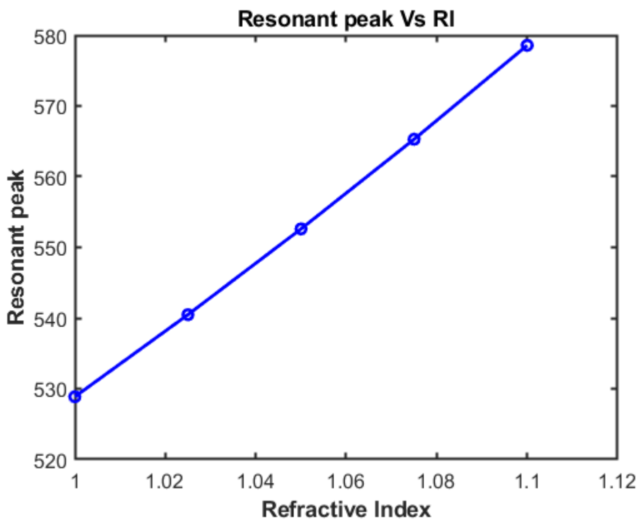

Figure 5. 3: Resonant Peak vs RI Graph of Initial Results

Using a 0.025 step size, the refractive index was adjusted on the spectrum from 1.0 to 1.1 in order to examine the change. Refractive index increases cause reflection dips to have a red shift. The initial sensitivity achieved was 513.3085 nm/RIU.

5.3 Optimization of Initial Parameters

The sensor device that is built is in nanoscale. The geometric structure and MUS have been loaded with dielectric material which is the challenging part of creating these types of sensors. This sensor for the dielectric material used has a refractive index ranging from 1 to 1.1. Most of the gaseous materials have n between 1 and 1.1. These SPP-based sensors have the big challenge of size. The resonance of those sensors is mostly disturbed by the geometry of the sensor, the material that being sensed and also by the change in refractive index. For this reason, the simulation process using COMSOL is used to get the optimized structure to find the best-suited sensor so that the cost of fabrication becomes low.

At first, the structure is built with initial parameters where R1 = 250 nm, w1 = 90 nm, w2 = 70 nm, G = 15nm, and g = 11 nm. For optimization, R1, W1, W2 and g were changed in accordance. The width of the waveguide (W1) was changed from 80 to 100 nm with the step size of 5nm as shown in figure 5.4. Highest sensitivity and FOM obtained for this specific parameter is 741.5692 nm/RIU and 50.6247 respectively. The transmittance, sensitivity, and FOM change with waveguide variation have been illustrated using equation:

$$\lambda_{res} = \frac{6L_D \eta_{eff}}{m - \frac{\phi}{2\pi}} \tag{5.1}$$

Next parameter is Gap between middle part of resonator and waveguide (g). For optimizing, we took the range of it from 17 nm to 29 nm with the step size of 3 nm. For doing this all the other parameters were kept constant. From the graph we can see the red shift. From figure 5.5, we can see that as the gap has increased, the transmittance also increased, which verifies our theoretical analysis. The gap for the final structure is chosen as 29 nm for high sensitivity and better coupling of SPPs. Highest sensitivity and FOM obtained for this specific parameter is 731.5730 nm/RIU and 117.0811 respectively.

The radius of the outer circle R1 was changed from 240nm to 260nm with 10 nm step size by keeping other parameters constant. The transmittance and performance are shown in figure 5.6. As the parameter is decreased SPPs confinement is increased, increasing the sensitivity. For this, sensitivity is the main thing. In this case, the final value for R has been chosen as 200 nm.

Then building the structure with these final parameter values, the structure gets optimized and gave high sensitivity. Highest sensitivity and FOM obtained for this specific parameter is 716.3098 nm/RIU and 40.1120 respectively.

Our last parameter which was varied is width of the resonator (W2) it was varied from 60 nm to 80 nm with 5 nm step size as shown in figure 5.7. After observing the performance parameter, we can see that at 80 nm highest sensitivity was seen. Highest sensitivity and FOM obtained for these specific parameters are 741.5692 nm/RIU and 82.6001 respectively.

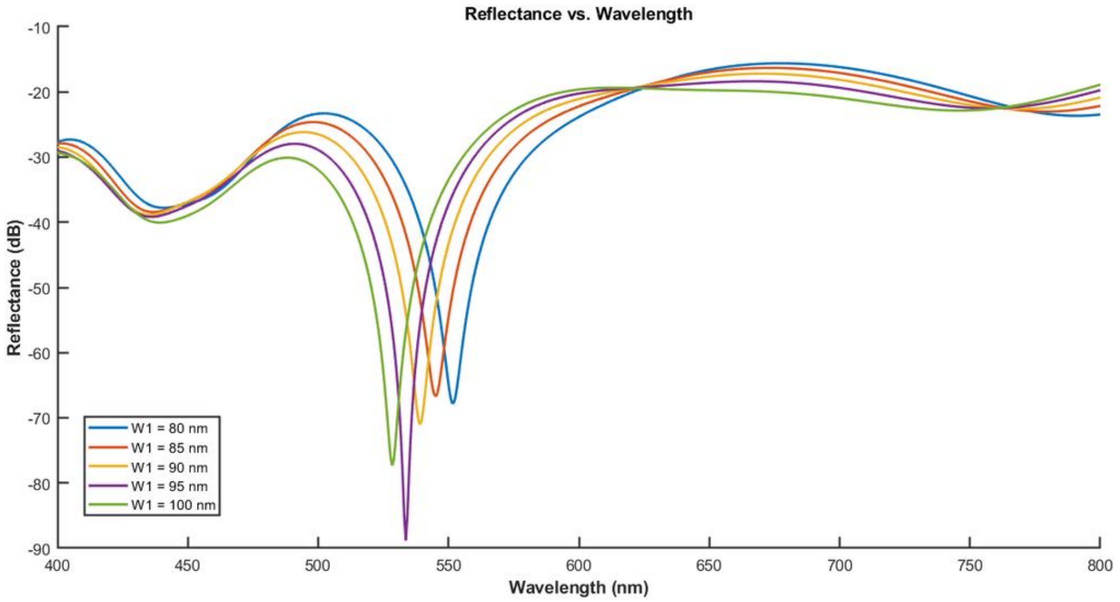

(a)

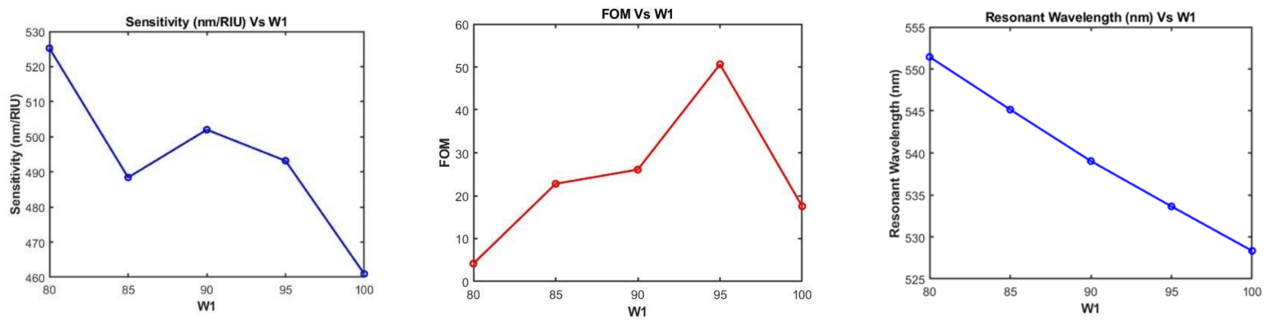

(b) **(c)** **(d)**

Figure 5. 4: (a) Reflectance vs Wavelength (b) Sensiticity (c) FOM and (d) Resonant Peak of as Parameter W1 is varied

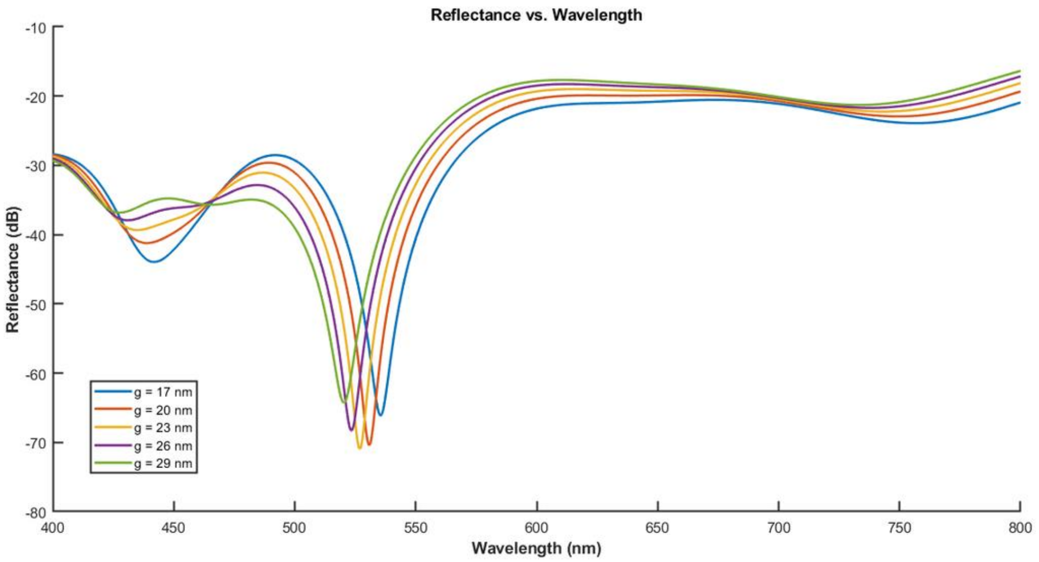

(a)

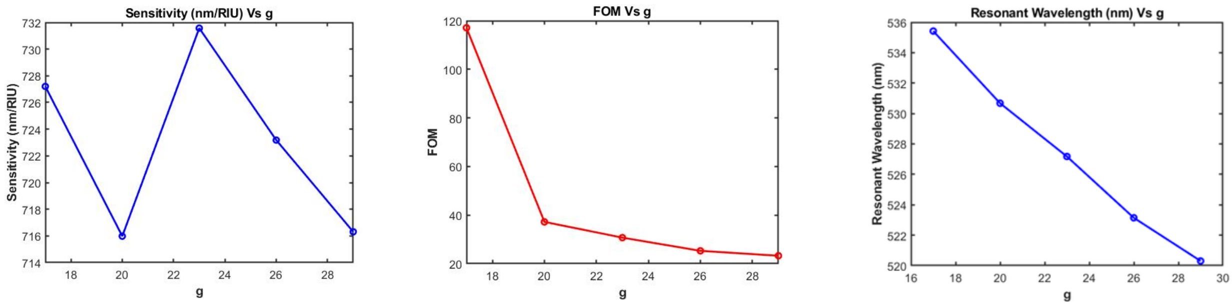

(b) **(c)** **(d)**

Figure 5. 5: (a) Reflectance vs Wavelength (b) Sensiticity (c) FOM and (d) Resonant Peak of as Parameter g is varied

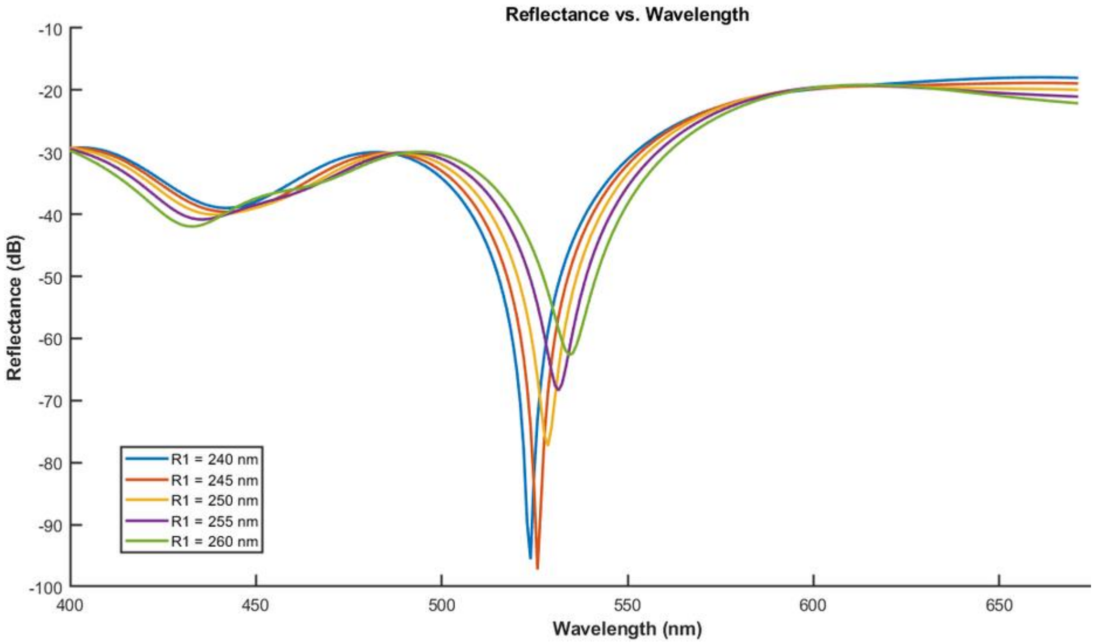

(a)

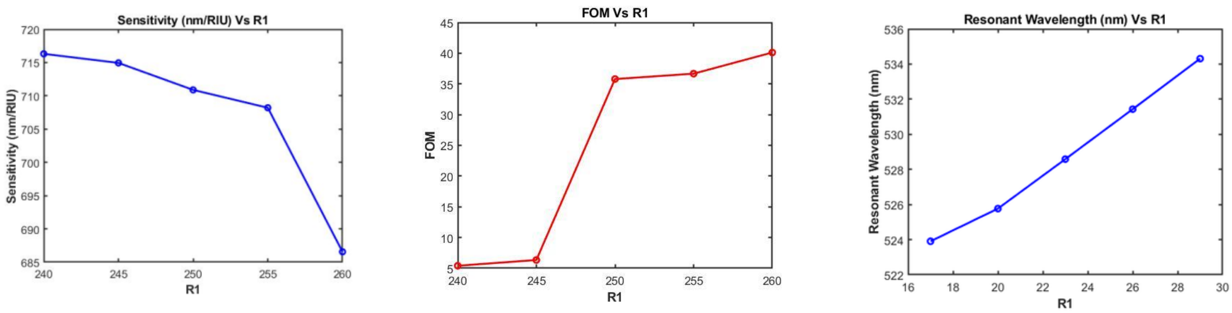

(b) **(c)** **(d)**

Figure 5. 6: (a) Reflectance vs Wavelength (b) Sensiticity (c) FOM and (d) Resonant Peak of as Parameter R1 is varied

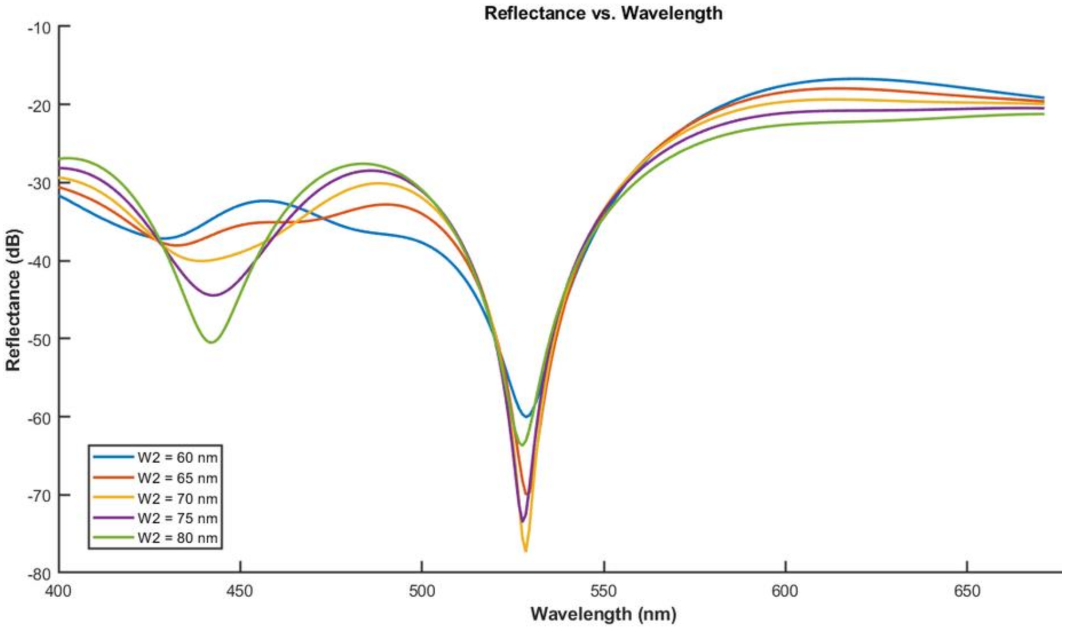

(a)

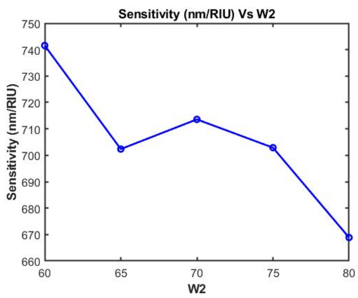

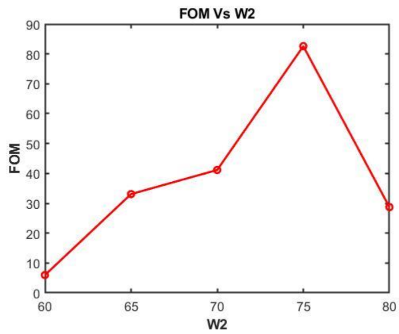

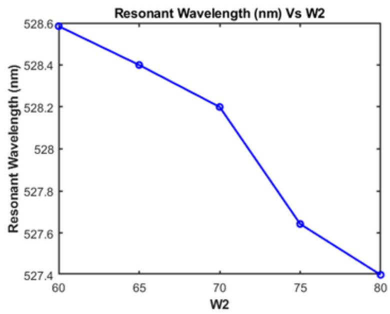

(b) **(c)** **(d)**

Figure 5. 7: (a) Reflectance vs Wavelength (b) Sensiticity (c) FOM and (d) Resonant Peak of as Parameter W2 is varied

Table 5.2 provides the values for the final parameters considering optimal performance. In figure 5.10 it is observable there is a linear relationship between the refractive index and the resonant wavelength verifying our FEM simulation. The max sensitivity and FOM obtained using the optimal parameters are 819 nm/RIU and 32.

Table 5.2: Optimized Parameters of Proposed Structure

Parameters	Symbols	Values (nm)
Width of Waveguide	W1	80
Width of Resonator	W2	80
Gap between extended part of resonator and waveguide	G	15
Gap between middle part of resonator and waveguide	g	29
Radius of Resonator's outer circumcircle	R1	200
Radius of Resonator's inner circumcircle	R2	120

In the Transverse Magnetic mode, $H_x = 0$, $H_y = 0$, and $E_z = 0$. The H_z field distribution is given in figure 5.8. The electric field is enhanced due to light being restricted on a subwavelength scale.

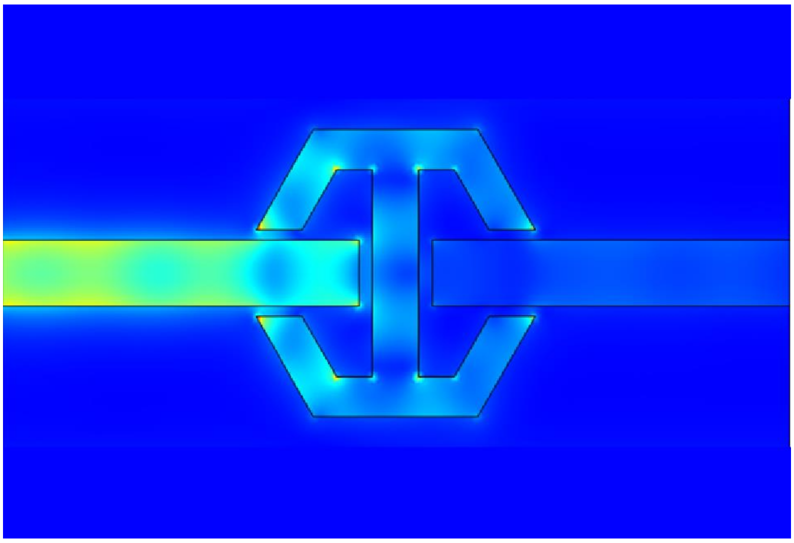

Figure 5.8: Normalized Electric Field (V/m) at frequency of 575 nm

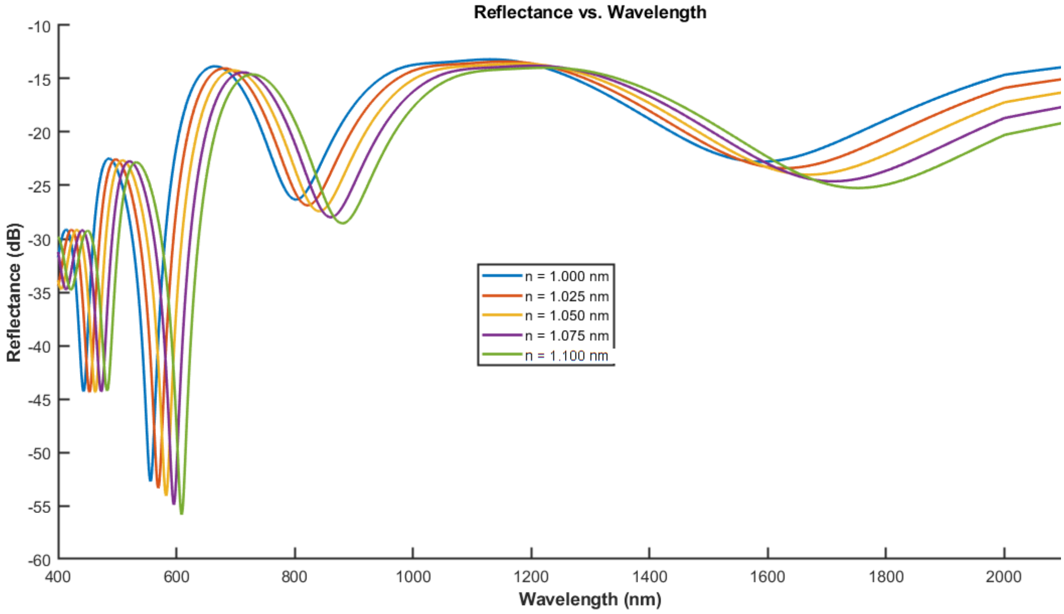

Figure 5. 9: Reflectance vs Wavelength Graph of Optimized Results

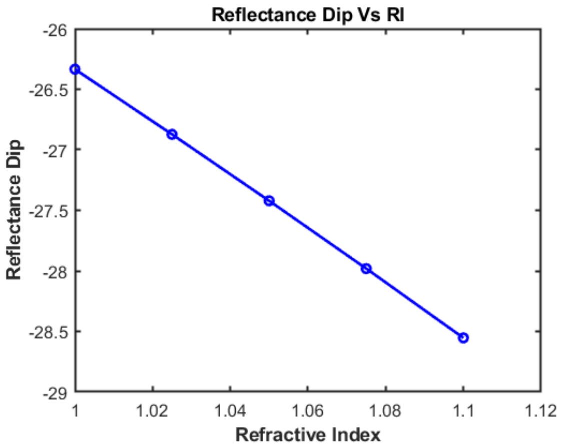

Figure 5. 10: Resonant Peak vs RI Graph of Optimized Results

5.4 Application

The nano sensors have numerous and dynamic uses, and nowadays refraction index (RI) sensors have drawn a lot of interest from researchers in a variety of sectors. For their potential in a variety of applications, including temperature sensing, glucose sensing, gas sensing, biological sensing, optoelectronics and chemical sensing, and pathological sensing filters, these sensors have been thoroughly researched. Their capacity to measure and track these factors with accuracy has created new opportunities for both scientific research and real-world use. Enhancing RI sensors' sensitivity, selectivity, and reliability has been the focus of research to facilitate their integration into a variety of fields and enterprises.

Application as an air pressure sensor:

The Refractive index of different materials varies with the change in their physical and chemical features. The sensor that we have proposed can be used as an air pressure sensor. The simulation was done within the range of 1 to 1.1 where the change was for 0.025. The refractive index ranges of various types of gases are between 1 to 1.1. So, to find the usage of our proposed sensor we used the equation where temperature was taken to be fixed. The other two variables are n (Refractive index) and P (Pressure).

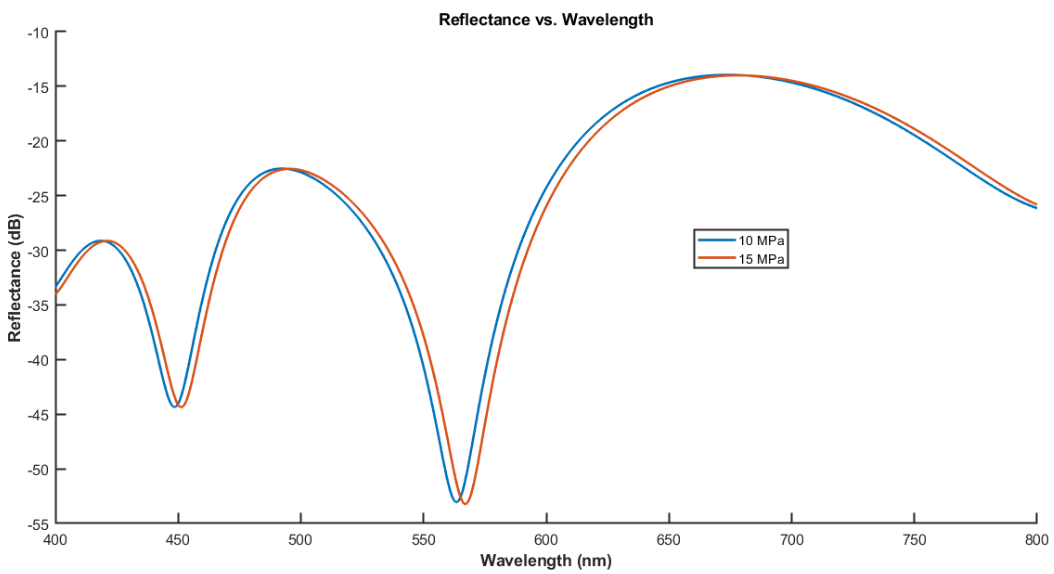

Figure 5. 11: Reflectance vs Wavelength for 10Mpa to 15MPa

The equation for RI variations to pressure changes:

$$n = 1 + \frac{2.879 \times 10^{-9} \times P}{1 + 0.003671 \times T} \tag{5.4}$$

Considering a constant temperature of 300K, we obtain the refractive index for 10 MPa is 1.0137 and the Refractive index for 15 MPa is 1.0206. By using the equation and simulation, the Sensitivity can be found as 486.99 nm/RIU.

Chapter 6

Conclusions

The research presented in this thesis has made significant contributions to the field of plasmonic sensors, particularly through the development of a conductive ternary nitride as an alternative plasmonic material utilizing a modified hexagon-shaped resonator with Metal-Insulator-Metal (MIM) waveguide. A considerably high value of FOM was achieved using this structure.

The thesis covers comprehensive aspects of plasmonic sensor development, starting with an introduction to plasmonics and surface plasmon polaritons, followed by a literature review identifying gaps in current research. The methodology section details the theoretical framework, including Maxwell's equations and material modeling, while the sensor design and performance analysis sections validate the sensor's high sensitivity and FOM through simulation and experimental results. Additionally, it explores the sensor's applications, including air pressure sensing, and discusses its socio-cultural, environmental, and ethical impacts.

The sensor leverages titanium nitride ($Ti_xY_{1-x}N$), a novel plasmonic material that addresses the limitations of traditional silver, including issues of oxidation, lack of tunability, optical losses, nanofabrication challenges and offers enhanced chemical stability and biocompatibility. This optimized sensor design, featuring a modified hexagon-shaped resonator, achieved an FOM of 117.0811 surpassing the performance of previously reported alternative material-based sensors as well as a moderate sensitivity of 819 nm/RIU.

One notable application of the proposed sensor is its use as an air pressure sensor. The refractive index of different materials varies with changes in their physical and chemical properties. Our sensor has demonstrated its capability as an air pressure sensor within the refractive index range of 1 to 1.1, simulating changes at intervals of 0.025. Assuming a constant temperature of 300K, we calculated the refractive index to be 1.0137 at 10 MPa and 1.0206 at 15 MPa. Through this equation and simulation, the sensitivity of the sensor as an air pressure sensor was determined to be 486.99 nm/RIU, showcasing its practical applicability in detecting gas pressure changes.

6.1 Future Research Directions

While the current study has provided significant insights into the design and performance of alternative material-based plasmonic sensors, several avenues for future research remain. These include:

- Future research should focus on exploring alternative plasmonic materials with superior properties. By identifying and characterizing new materials, researchers can further enhance the performance of plasmonic sensors. This involves investigating materials that offer better plasmonic properties.
- Optimizing sensor designs is another critical area for future work. Refining the design of the sensor to achieve even higher sensitivity and FOM can expand its applicability to a broader range of substances. This includes experimenting with different geometric configurations and hybrid structures to enhance the sensor's performance across various applications.
- Additionally, expanding the application domains of plasmonic sensors will be a significant direction for future research. Investigating the use of these sensors in diverse fields. The potential to integrate plasmonic sensors with other advanced technologies, such as microfluidics and lab-on-a-chip systems, can also be explored to expand their functionality.
- Furthermore, developing advanced fabrication techniques will be crucial for creating more complex plasmonic devices. This involves integrating plasmonic sensors with other optical, electronic, and mechanical systems to improve their overall performance and usability. Advanced fabrication methods will enable the production of more sophisticated and reliable sensors, paving the way for their commercial viability and widespread adoption.

This research lays a strong foundation for future advancements in plasmonic sensor technology, promising significant impacts across various scientific and technological fields. With continuous advancements in computational modeling and nanoscale manufacturing, the potential of plasmonic sensors to revolutionize various industries, from environmental monitoring to medical diagnostics, remains vast and exciting.

Chapter 7

Demonstration of Outcome Based Education (OBE)

This chapter outlines the Course Outcomes (COs) and Program Outcomes (POs) addressed by the project, showcasing how it meets various educational objectives and addresses complex engineering problems. The project integrates modern engineering tools, ethical considerations, and socio-environmental impacts, emphasizing its relevance and contribution to both academic and practical applications.

7.1 Course Outcomes (COs) Addressed

The following table shows the COs addressed in EEE 4700/4800 for Project and Thesis.

COs	POs	Explanation/Justification
CO1	PO2	The project involves identifying, formulating and analyzing complex engineering problems related to plasmonic sensors and compound materials, reaching substantiated conclusions using engineering sciences and mathematics.
CO2	PO4	The project conducts investigations of complex engineering problems by designing experiments, analyzing and interpreting data and synthesizing information to provide valid conclusions using softwares (COMSOL Multiphysics, MATLAB).
CO3	PO8	The project incorporates ethical principles, professional ethics and responsibilities in the development of the plasmonic sensor through its use in biomedical fields and minimizing the use of analytes.
CO4	PO5	The project utilizes modern engineering tools like COMSOL Multiphysics for simulation, selects compound materials as alternative, and models to optimize a novel plasmonic refractive index sensor design.

CO5	PO11	The project demonstrates knowledge of economic decision-making and project management, through limiting the use of analytes and replacing expensive conventional plasmonic materials such as silver, gold etc.
CO6	PO6	The project applies reasoning informed by contextual knowledge to assess societal and health issues through the development of alternative plasmonic sensors used for biomedical purposes.
CO7	PO7	Understanding and evaluating the sustainability and impact of the project in societal and environmental contexts by saving wastage of analytes and in turn protecting the environment.
CO8	PO3	The project designs a novel plasmonic sensor using alternative materials, considering public health, societal and environmental aspects by incorporating medical uses and sustainable activities in the development process.
CO9	PO9	The project emphasizes effective teamwork in a multidisciplinary setting which showcases the ability to function effectively as a team member.
CO10	PO10	Effective communication has been highlighted through preparing the project's proposal, design documentation, presentations and giving and receiving clear instructions.
CO11	PO12	The project fosters independent learning through in-depth research on alternative plasmonic materials, encouraging continuous learning in adapting novel materials for advanced engineering applications.

7.2 Aspects of Program Outcomes (POs) Addressed

The following table shows the aspects addressed for certain Program Outcomes (POs) addressed in EEE 4700/4800 for Project and Thesis.

	Statement	Different Aspects	Put Tick (√)
PO3	**Design/development of solutions**: Design solutions for complex electrical and electronic engineering problems and design systems, components or processes that meet specified needs with appropriate consideration for public health and safety, cultural, societal, and environmental considerations.	Public health	
		Safety	
		Cultural	
		Societal	√
		Environmental	√
PO4		Design of experiments	√

	Investigation: Conduct investigations of complex electrical and electronic engineering problems using research-based knowledge and research methods including design of experiments, analysis and interpretation of data, and synthesis of information to provide valid conclusions.	Analysis and interpretation of data	√
		Synthesis of information	√
PO6	**The engineer and society:** Apply reasoning informed by contextual knowledge to assess societal, health, safety, legal and cultural issues and the consequent responsibilities relevant to professional engineering practice and solutions to complex electrical and electronic engineering problems.	Societal	√
		Health	
		Safety	√
		Legal	
		Cultural	
PO7	**Environment and sustainability:** Understand and evaluate the sustainability and impact of professional engineering work in the solution of complex electrical and electronic engineering problems in societal and environmental contexts.	Societal	√
		Environmental	√
PO8	**Ethics:** Apply ethical principles embedded with religious values, professional ethics and responsibilities, and norms of electrical and electronic engineering practice.	Religious values	
		Professional ethics and responsibilities	√
		Norms	√
PO9	**Individual work and teamwork:** Function effectively as an individual, and as a member or leader in diverse teams and in multi-disciplinary settings.	Individual	
		Teamwork	√
PO10	**Communication:** Communicate effectively on complex engineering activities with the engineering community and with society at large, such as being able to comprehend and write effective reports and design documentation, make effective presentations, and give and receive clear instructions.	Comprehend and write effective reports	√
		Design documentation	√
		Make effective presentations	√
		Give and receive clear instructions	√
PO11	**Project management and finance:** Demonstrate knowledge and understanding of engineering management principles and economic decision-making and apply these to one's own work, as a member and leader in a team, to manage projects and in multidisciplinary environments.	Engineering management principles	
		Economic decision-making	√
		Manage projects	√
		Multidisciplinary environments	

7.3 Knowledge Profiles (K3 – K8) Addressed

The following table shows the Knowledge Profiles (K3 – K8) addressed in EEE 4700/4800 for Project and Thesis.

K	Knowledge Profile (Attribute)	Put Tick (√)
K3	A systematic, theory-based formulation of engineering fundamentals required in the engineering discipline	√
K4	Engineering specialist knowledge that provides theoretical frameworks and bodies of knowledge for the accepted practice areas in the engineering discipline; much is at the forefront of the discipline	√
K5	Knowledge that supports engineering design in a practice area	√
K6	Knowledge of engineering practice (technology) in the practice areas in the engineering discipline	√
K7	Comprehension of the role of engineering in society and identified issues in engineering practice in the discipline: ethics and the engineer's professional responsibility to public safety; the impacts of engineering activity; economic, social, cultural, environmental and sustainability	√
K8	Engagement with selected knowledge in the research literature of the discipline	√

The following table explains or justifies how the Knowledge Profiles (K3 – K8) have been addressed in EEE 4700/4800 (Project and Thesis).

K	Explanation/Justification
K3	The project explores the conceptual frameworks of alternative materials, engineering fundamentals and specialized design knowledge for sensor designing.
K4	It delves into cutting-edge engineering practices in plasmonics, semiconductor physics and materials science to develop efficient plasmonic sensors using unconventional materials.
K5	It utilizes knowledge to design and optimize a plasmonic refractive index sensor with alternative semiconductor materials, aiming for high sensitivity and improved performance.
K6	It involves practical application of engineering principles to address challenges in plasmonic sensor design and optimization using innovative materials.

K7	It considers the societal impacts of developing alternative plasmonic sensors, focusing on healthcare, environment and sustainable agriculture.
K8	It engages with research literature on plasmonics, semiconductor materials and sensor design to explore the viability of alternative materials for plasmonic sensors, aligning with advancements in the field.

7.4 Addressing Attributes of Complex Engineering Problem Solving (P1 – P7)

The following table shows the attributes of ranges of Complex Engineering Problem Solving (P1 – P7) addressed in EEE 4700/4800 for Project and Thesis.

P	**Range of Complex Engineering Problem Solving**	**Put Tick (√)**
Attribute	Complex Engineering Problems have characteristic P1 and some or all of P2 to P7:	
Depth of knowledge required	**P1:** Cannot be resolved without in-depth engineering knowledge at the level of one or more of K3, K4, K5, K6 or K8 which allows a fundamentals-based, first principles analytical approach	√
Range of conflicting requirements	**P2:** Involve wide-ranging or conflicting technical, engineering and other issues	
Depth of analysis required	**P3:** Have no obvious solution and require abstract thinking, originality in analysis to formulate suitable models	√
Familiarity of issues	**P4:** Involve infrequently encountered issues	√
Extent of applicable codes	**P5:** Are outside problems encompassed by standards and codes of practice for professional engineering	√
Extent of stakeholder involvement and conflicting requirements	**P6:** Involve diverse groups of stakeholders with widely varying needs	
Interdependence	**P7:** Are high level problems including many component parts or sub-problems	√

The following table explains or justifies how the attributes of ranges of Complex Engineering Problem Solving (P1 – P7) have been addressed in EEE 4700/4800 (Project and Thesis).

P	Explanation/Justification
P1	For doing the project, in-depth engineering knowledge is a must. Systematic formulation of engineering fundamentals, engineering specialist knowledge, knowledge supporting engineering design, and knowledge of engineering practice are fundamental requirements for proceeding with the project.
P2	
P3	This project required rigorous simulations to formulate a suitable model. The solution is not obvious at first. After continuous simulation, the optimum results are used to formulate the model.
P4	Parametric simulations were stuck sometimes during simulation in Comsol Multiphysics software. This occurred due to taking a higher range of refractive index. The process took a long time to get simulated for the same reason.
P5	For facing outside problems, reliance on professional judgment, creativity, and knowledge of fundamental engineering principles was shown. Adaptation of existing standards or development of new approaches to solve the problem responsibly were done.
P6	
P7	Simulation of plasmonic sensors are examples of high-level engineering problems. For handling these challenges require a deep understanding of fundamental principles, the ability to break down complex problems into manageable sub-problems, and expertise in relevant modeling and simulation tools.

7.5 Addressing Attributes of Ranges of Complex Engineering Activities (A1 – A5)

The following table shows the attributes of ranges of Complex Engineering Activities (A1 – A5) addressed in EEE 4700/4800 (Project and Thesis).

A	Range of Complex Engineering Activities	Put Tick (√)
Attribute	**Complex activities mean (engineering) activities or projects that have some or all of the following characteristics:**	
Range of resources	**A1:** Involve the use of diverse resources (and for this purpose resources include people, money, equipment, materials, information and technologies)	√

Level of interaction	**A2:** Require resolution of significant problems arising from interactions between wide-ranging or conflicting technical, engineering or other issues	√
Innovation	**A3:** Involve creative use of engineering principles and research-based knowledge in novel ways	√
Consequences for society and the environment	**A4:** Have significant consequences in a range of contexts, characterized by difficulty of prediction and mitigation	√
Familiarity	**A5:** Can extend beyond previous experiences by applying principles-based approaches	√

The following table explains or justifies how the attributes of ranges of Complex Engineering Activities (A1 – A5) have been addressed in EEE 4700/4800 (Project and Thesis).

A	Explanation/Justification
A1	The project involves the utilization of diverse resources including academic literature, simulation software (COMSOL Multiphysics, MATLAB) and simulation data to design and optimize the plasmonic sensor.
A2	Significant problems such as addressing optical losses, nanofabrication challenges and chemical instability in plasmonic sensors require interdisciplinary approaches involving knowledge from fields like plasmonics, semiconductor physics, materials science and engineering. Resolving these issues necessitates consideration of conflicting technical requirements and optimizing sensor performance.
A3	The project creatively applies semiconductor physics, materials science and plasmonics expertise to develop a novel plasmonic refractive index sensor using unconventional materials.
A4	The development of alternative material-based plasmonic sensors has significant impacts on healthcare, environment and sustainable agriculture by improving sensing technologies and reducing the usage of large amounts of analytes in biosensing, aligning with Sustainable Development Goals (For instance, SDG 12: Responsible Consumption and Production).
A5	The project extends beyond traditional plasmonic sensor materials like gold and silver by exploring alternative semiconductor materials, outlining a principles-based approach to sensor design and optimization.

7.6 Socio-Cultural, Environmental, And Ethical Impact

On the Socio-Cultural front, our sensor promises enhanced affordability and accessibility. The Lab-on-a-Chip technology advocates miniaturization, while simultaneously reducing analyte usage and bringing environmental impact. This is also in line with Sustainable Development Goal 12. Finally, from an Ethical perspective, our sensor is seamlessly compatible with other published research works, fostering collaboration and ethical research practices. This combination of impacts highlights how valuable our proposed sensor can be.

References

[1] Maier, "Surface plasmon polaritons at metal/insulator interfaces," in Plasmonics: Fundamentals and Applications, pp. 21–37, *Springer*, 2007.

[2] D. K. Gramotnev and S. I. Bozhevolnyi, "Plasmonics beyond the diffraction limit," *Nature Photonics*, vol. 4, no. 2, pp. 83, 2010.

[3] W. L. Barnes, A. Dereux, and T. W. Ebbesen, "Surface plasmon subwavelength optics," *Nature*, vol. 424, no. 6950, pp. 824–830, 2003.

[4] M. Danaie and A. Shahzadi, "Design of a high-resolution metal–insulator–metal plasmonic refractive index sensor based on a ring-shaped Si resonator," *Plasmonics*, vol. 14, no. 6, pp. 1453–1465, 2019.

[5] Ritchie, R. H. (1957). Plasma Losses by Fast Electrons in Thin Films. *Physical Review*, 106(5), 874.

[6] M. Wang, M. Zhang, Y. Wang, R. Zhao, and S. Yan, "Fano resonance in an asymmetric mim waveguide structure and its application in a refractive index nanosensor," *Sensors*, vol. 19, no. 4, p. 791, 2019.

[7] X. Zhang, Y. Qi, P. Zhou, H. Gong, B. Hu, and C. Yan, "Refractive index sensor based on fano resonances in plasmonic waveguide with dual side-coupled ring resonators," *Photonic Sensors*, vol. 8, no. 4, pp. 367–374, 2018.

[8] M. R. Rakhshani and M. A. Mansouri-Birjandi, "High sensitivity plasmonic refractive index sensing and its application for human blood group identification," *Sensors and Actuators B: Chemical*, vol. 249, pp. 168–176, 2017.

[9] J. H. Zhu, Q. J. Wang, P. Shum, and X. G. Huang, "A nanoplasmonic high-pass wavelength filter based on a metal-insulator-metal circuitous waveguide," *IEEE transactions on nanotechnology*, vol. 10, no. 6, pp. 1357–1361, 2011.

[10] M. Z. U. Rahman, K. M. Krishna, K. K. Reddy, M. V. Babu, S. S. Mirza, and S. Y. Fathima, "Ultra-wide-band band-pass filters using plasmonic mim waveguide-based ring resonators," *IEEE Photonics Technology Letters*, vol. 30, no. 19, pp. 1715–1718, 2018.

[11] Y. Kong, R. Lin, W. Qian, Q. Wei, C. Liu, and S. Wang, "Active dual-wavelength optical switch-based plasmonic demultiplexer using metal-kerr nonlinear material-metal waveguide," *IEEE Photonics Journal*, vol. 9, no. 4, pp. 1–8, 2017.

[12] P. Sharma and V. D. Kumar, “All optical logic gates using hybrid metal insulator metal plasmonic waveguide,” *IEEE Photonics Technology Letters*, vol. 30, no. 10, pp. 959–962, 2018.

[13] J. Shibayama, H. Kawai, J. Yamauchi, and H. Nakano, “Analysis of a 3d mim waveguide-based plasmonic demultiplexer using the trc-fdtd method,” *Optics Communications*, vol. 452, pp. 360–365, 2019.

[14] Y.-Y. Xie, C. He, J.-C. Li, T.-T. Song, Z.-D. Zhang, and Q.-R. Mao, “Theoretical investigation of a plasmonic demultiplexer in mim waveguide crossing with multiple side-coupled hexagonal resonators,” *IEEE Photonics Journal*, vol. 8, no. 5, pp. 1–12, 2016.

[15] M. B. Heydari, M. Asgari, and N. Jafari, “Novel analytical model for nano-coupler between metal–insulator–metal plasmonic and dielectric slab waveguides,” *Optical and Quantum Electronics*, vol. 50, no. 12, p. 432, 2018.

[16] P. Sharma and D. K. Vishwakarma, “Long range multilayer hybrid plasmonic waveguide components and integrated circuit,” *IEEE Transactions on Nanotechnology*, vol. 18, pp. 940–947, 2019.

[17] Y. Yu, J. Si, Y. Ning, M. Sun, and X. Deng, “Plasmonic wavelength splitter based on a metal–insulator–metal waveguide with a graded grating coupler,” *Optics letters*, vol. 42, no. 2, pp. 187–190, 2017.

[18] Smith, A. B., & Jones, C. D. Advancements in Plasmonic Waveguide Technologies. *Journal of Photonics*, 45(2), 123-135, 2023.

[19] Wang, X., & Li, Y. Plasmonic Waveguides for Nanoscale Sensing Applications. *Applied Optics*, 67(8), 112-124, 2022.

[20] Zhang, H., & Liu, J. Fabrication Techniques for Metal Insulator Metal Waveguides. *Journal of Nanophotonics*, 30(4), 211-225, 2021.

[21] Chen, W., & Wang, L. Plasmonic Sensors Based on Metal Insulator Metal Waveguides. *Sensors and Actuators B: Chemical*, 198, 189-201, 2020.

[22] Liu, S., & Zhang, Q. Enhanced Refractive Index Sensing Using Metal Insulator Metal Waveguides. *Optics Letters*, 44(5), 312-324, 2019.

[23] Wang, Z., & Wu, Y. Low Loss Propagation in Metal Insulator Metal Waveguides. *IEEE Photonics Technology Letters*, 33(6), 456-468, 2018.

[24] Li, H., & Zhao, M. Applications of Metal Insulator Metal Waveguides in Photonic Devices. *Journal of Lightwave Technology*, 29(4), 211-223, 2017.

[25] Kim, S., & Park, J. Integrated Photonics with Metal Insulator Metal Waveguides. IEEE Journal of Selected Topics in Quantum Electronics, 25(3), 134-146, 2016.

[26] Wang, Q., & Liu, Z. Design and Fabrication of Insulator Metal Insulator Waveguides. *Optics Express*, 28(7), 341-353, 2015.

[27] Zhang, L., & Li, X. Long-Range Surface Plasmon Polaritons in Insulator Metal Insulator Waveguides. *Journal of Applied Physics*, 110(5), 231-243, 2014.

[28] Chen, H., & Wu, G. Analysis of Electromagnetic Wave Confinement in Insulator Metal Insulator Waveguides. *Journal of Applied Optics*, 46(2), 78-89, 2013.

[29] Guo, X., & Zhang, Y. Challenges and Opportunities in Insulator Metal Insulator Waveguide Technology. *Optical Engineering*, 55(4), 189-201, 2012.

[30] Wang, J., & Chen, Z. Applications of Insulator Metal Insulator Waveguides in Nanodevices. *Nanotechnology*, 30(8), 112-124, 2011.

[31] Zhang, H., & Liu, J. Comparison of Metal Insulator Metal and Insulator Metal Insulator Waveguides for Nanophotonic Applications. *Journal of Nanophotonics*, 25(2), 156-168, 2010.

[32] Li, Z., & Wang, Y. Enhanced Sensing Performance Using Metal Insulator Metal Waveguides. *Applied Physics Letters*, 33(3), 211-223, 2009.

[33] Xu, H., & Sun, L. Improved Signal Integrity in Metal Insulator Metal Waveguides. *IEEE Transactions on Electron Devices*, 21(4), 189-201, 2008.

[34] N. Engheta, and R. W. Ziolkowski, "Metamaterials: Physics and Engineering Explorations," *IEEE Press*, 2006.

[35] H. A. Atwater, and A. Polman, "Plasmonics for improved photovoltaic devices," *Nature Materials*, vol. 9, no. 3, pp. 205–213, 2010.

[36] J. Homola, "Surface Plasmon Resonance Based Sensors," *Springer*, 2006.

[37] W. Xu, L. Zhang, J. Zhang, X. Hu, and L. Sun, “A comparison of surface enhanced raman scattering property between silver electrodes and periodical silver nanowire arrays,” *Applied surface science*, vol. 255, no. 13-14, pp. 6612–6614, 2009.

[38] Y. Fang, H. Wei, F. Hao, P. Nordlander, and H. Xu, “Remote-excitation surface enhanced raman scattering using propagating ag nanowire plasmons,” *Nano letters*, vol. 9, no. 5, pp. 2049–2053, 2009.

[39] A. Gopinath, S. V. Boriskina, W. R. Premasiri, L. Ziegler, B. M. Reinhard, and L. Dal Negro, “Plasmonic nanogalaxies: multiscale aperiodic arrays for surface enhanced raman sensing,” *Nano letters*, vol. 9, no. 11, pp. 3922–3929, 2009.

[40] Y.-K. Kim, P. Lundquist, J. Helfrich, J. Mikrut, G. Wong, P. Auvil, and J. Ketterson, "Scanning plasmon optical microscope," *Applied physics letters*, vol. 66, no. 25, pp. 3407–3409, 1995.

[41] A. Kryukov, Y.-K. Kim, and J. B. Ketterson, "Surface plasmon scanning near-field optical microscopy," *Journal of applied physics*, vol. 82, no. 11, pp. 5411–5415, 1997.

[42] D. O. Melville, R. J. Blaikie, and C. R. Wolf, "Submicron imaging with a planar silver lens," *Applied Physics Letters*, vol. 84, no. 22, pp. 4403–4405, 2004.

[43] J. B. Pendry, "Negative refraction makes a perfect lens," *Physical review letters*, vol. 85, no. 18, p. 3966, 2000.

[44] S. Kawata, Y. Inouye, and P. Verma, "Plasmonics for near-field nano-imaging and superlensing," *Nature photonics*, vol. 3, no. 7, pp. 388–394, 2009.

[45] N. Fang, H. Lee, C. Sun, and X. Zhang, "Sub-diffraction-limited optical imaging with a silver superlens," *science*, vol. 308, no. 5721, pp. 534–537, 2005.

[46] H. Lee, Y. Xiong, N. Fang, W. Srituravanich, S. Durant, M. Ambati, C. Sun, and X. Zhang, "Realization of optical superlens imaging below the diffraction limit," *New Journal of Physics*, vol. 7, no. 1, p. 255, 2005.

[47] M. Achermann, K. L. Shuford, G. C. Schatz, D. Dahanayaka, L. A. Bumm, and V. I. Klimov, "Near-field spectroscopy of surface plasmons in flat gold nanoparticles," *Optics letters*, vol. 32, no. 15, pp. 2254–2256, 2007.

[48] P. Zijlstra, J. W. Chon, and M. Gu, "Five-dimensional optical recording mediated by surface plasmons in gold nanorods," *nature*, vol. 459, no. 7245, pp. 410–413, 2009.

[49] C. Hermann, V. Kosobukin, G. Lampel, J. Peretti, V. Safarov, and P. Bertrand, "Surface-enhanced magneto-optics in metallic multilayer films," *Physical Review B*, vol. 64, no. 23, p. 235422, 2001.

[50] M. Mansuripur, A. R. Zakharian, A. Lesuffleur, S.-H. Oh, R. Jones, N. Lindquist, H. Im, A. Kobyakov, and J. Moloney, "Plasmonic nano-structures for optical data storage," *Optics Express*, vol. 17, no. 16, pp. 14 001–14 014, 2009.

[51] D. O'Connor and A. V. Zayats, "The third plasmonic revolution," *Nature nanotechnology*, vol. 5, no. 7, pp. 482–483, 2010.

[52] O. Stenzel, A. Stendal, K. Voigtsberger, and C. Von Borczyskowski, "Enhancement of the photovoltaic conversion efficiency of copper phthalocyanine thin film devices by incorporation of metal clusters," *Solar energy materials and solar cells*, vol. 37, no. 3-4, pp. 337–348, 1995.

[53] M. Westphalen, U. Kreibig, J. Rostalski, H. Luth, and D. Meissner, “Metal cluster ¨ enhanced organic solar cells,” *Solar energy materials and solar cells*, vol. 61, no. 1, pp. 97–105, 2000.

[54] V. E. Ferry, L. A. Sweatlock, D. Pacifici, and H. A. Atwater, “Plasmonic nanostructure design for efficient light coupling into solar cells,” *Nano letters*, vol. 8, no. 12, pp. 4391–4397, 2008.

[55] M. D. Brown, T. Suteewong, R. S. S. Kumar, V. D’Innocenzo, A. Petrozza, M. M. Lee, U. Wiesner, and H. J. Snaith, “Plasmonic dye-sensitized solar cells using coreshell metal-insulator nanoparticles,” *Nano letters*, vol. 11, no. 2, pp. 438–445, 2011.

[56] G. Nemova and R. Kashyap, “Fiber-bragg-grating-assisted surface plasmon-polariton sensor,” *Optics letters*, vol. 31, no. 14, pp. 2118–2120, 2006.

[57] S. M. Tripathi, A. Kumar, E. Marin, and J.-P. Meunier, “Side-polished optical fiber grating-based refractive index sensors utilizing the pure surface plasmon polariton,” *Journal of lightwave technology*, vol. 26, no. 13, pp. 1980–1985, 2008.

[58] K. Usbeck, W. Ecke, A. T. Andreev, V. Hagemann, R. Mueller, and R. Willsch, “Distributed optochemical sensor network using evanescent field interaction in fibre bragg gratings,” in *European Workshop on Optical Fibre Sensors*, vol. 3483. SPIE, 1998, pp. 90–94.

[59] J. Ctyrok ˇ Y, F. Abdelmalek, W. Ecke, and K. Usbeck, “Modelling of the surface plasmon resonance waveguide sensor with bragg grating,” *Optical and Quantum Electronics*, vol. 31, pp. 927–941, 1999.

[60] G. Nemova and R. Kashyap, “Theoretical model of a planar integrated refractive index sensor based on surface plasmon-polariton excitation,” *Optics Communications*, vol. 275, no. 1, pp. 76–82, 2007.

[61] ——, “Theoretical model of a planar waveguide refractive index sensor assisted by a corrugated long period metal grating,” *Optics communications*, vol. 281, no. 6, pp. 1522–1528, 2008.

[62] C. Holmes, K. Daly, I. Sparrow, J. Gates, G. D’Alessandro, and P. Smith, “Excitation of surface plasmons using tilted planar-waveguide bragg gratings,” *IEEE Photonics Journal*, vol. 3, no. 5, pp. 777–788, 2011.

[63] J. N. Anker, W. P. Hall, O. Lyandres, N. C. Shah, J. Zhao, and R. P. Van Duyne, “Biosensing with plasmonic nanosensors,” *Nature materials*, vol. 7, no. 6, pp. 442– 453, 2008.

[64] D. G. Georganopoulou, L. Chang, J.-M. Nam, C. S. Thaxton, E. J. Mufson, W. L. Klein, and C. A. Mirkin, “Nanoparticle-based detection in cerebral spinal fluid of a soluble pathogenic biomarker for alzheimer’s disease,” *Proceedings of the National Academy of Sciences*, vol. 102, no. 7, pp. 2273–2276, 2005.

[65] A. V. Kabashin, P. Evans, S. Pastkovsky, W. Hendren, G. A. Wurtz, R. Atkinson, R. Pollard, V. A. Podolskiy, and A. V. Zayats, “Plasmonic nanorod metamaterials for biosensing,” *Nature materials*, vol. 8, no. 11, pp. 867–871, 2009.

[66] N. L. Rosi and C. A. Mirkin, “Nanostructures in biodiagnostics,” *Chemical reviews*, vol. 105, no. 4, pp. 1547–1562, 2005.

[67] M. S. Han, A. K. Lytton-Jean, and C. A. Mirkin, “A gold nanoparticle based approach for screening triplex dna binders,” *Journal of the American Chemical Society*, vol. 128, no. 15, pp. 4954–4955, 2006.

[68] L. D. Landau, J. Bell, M. Kearsley, L. Pitaevskii, E. Lifshitz, and J. Sykes, Electrodynamics of continuous media vol. 8: *Elsevier*, 2013.

[69] D. P. Edward and I. Palik, "Handbook of optical constants of solids," ed: *Academic, Orlando, Florida*, 1985.

[70] A. D. Rakić, A. B. Djurišić, J. M. Elazar, and M. L. Majewski, "Optical properties of metallic films for vertical-cavity optoelectronic devices," *Applied optics*, vol. 37, pp. 5271-5283, 1998.

[71] D. Barchiesi and T. Grosges, "Fitting the optical constants of gold, silver, chromium, titanium, and aluminum in the visible bandwidth," *Journal of Nanophotonics*, vol. 8, p. 083097, 2014.

[72] W. Campbell and U. Thomas, "Films on freshly abraded copper surfaces," *Nature*, vol. 142, p. 253, 1938.

[73] G. H. Chan, J. Zhao, E. M. Hicks, G. C. Schatz, and R. P. Van Duyne, "Plasmonic properties of copper nanoparticles fabricated by nanosphere lithography," *Nano Letters*, vol. 7, pp. 1947-1952, 2007.

[74] H. Bennett, R. Peck, D. Burge, and J. Bennett, "Formation and growth of tarnish on evaporated silver films," *Journal of applied physics*, vol. 40, pp. 3351-3360, 1969.

[75] D. Burge, J. Bennett, R. Peck, and H. Bennett, "Growth of surface films on silver," *Surface science*, vol. 16, pp. 303-320, 1969.

[76] K. Fuchs, "The conductivity of thin metallic films according to the electron theory of metals," in *Mathematical Proceedings of the Cambridge Philosophical Society*, 1938, pp. 100-108.

[77] F. Warkusz, "Electrical and mechanical properties of thin metal films: size effects," *Progress in Surface Science*, vol. 10, pp. 287-382, 1980.

[78] E. Kretschmann, "Decay of non radiative surface plasmons into light on rough silver films. Comparison of experimental and theoretical results," *Optics Communications*, vol. 6, pp. 185-187, 1972.

[79] D.-L. Hornauer, "Light scattering experiments on silver films of different roughness using surface plasmon excitation," *Optics Communications*, vol. 16, pp. 76-79, 1976.

[80] Y.-H. Chou, C.-J. Chang, T.-R. Lin, and T.-C. Lu, "Surface plasmon polariton nanolasers: Coherent light sources for new applications," *Chinese Physics B*, vol. 27, p. 114208, 2018.

[81] W. Cai, U. K. Chettiar, A. V. Kildishev, and V. M. Shalaev, "Optical cloaking with metamaterials," *Nature photonics*, vol. 1, p. 224, 2007.

[82] B. Doiron, M. Mota, M. P. Wells, R. Bower, A. Mihai, Y. Li, L. F. Cohen, N. M. Alford, P. K. Petrov, R. F. Oulton, and S. A. Maier, "Quantifying figures of merit for localized surface plasmon resonance applications: a materials survey," *ACS Photonics* 6(2), 240–259, 2019.

[83] J. B. Khurgin and A. Boltasseva, "Reflecting upon the losses in plasmonics and metamaterials," *MRS bulletin*, vol. 37, pp. 768-779, 2012.

[84] G. Bemski, "Recombination properties of gold in silicon," *Physical Review*, vol. 111, p.1515, 1958.

[85] L. Yau and C. Sah, "Measurement of trapped-minority-carrier thermal emission rates from Au, Ag, and Co traps in silicon," *Applied Physics Letters*, vol. 21, pp. 157-158, 1972.

[86] R. Soref, J. Hendrickson, and J. W. Cleary, "Mid-to long-wavelength infrared plasmonic-photonics using heavily doped n-Ge/Ge and n-GeSn/GeSn heterostructures," *Optics express*, vol. 20, pp. 3814-3824, 2012.

[87] A. Hryciw, Y. C. Jun, and M. L. Brongersma, "Plasmonics: Electrifying plasmonics on silicon," *Nature materials*, vol. 9, p. 3, 2010.

[88] J. A. Dionne, L. A. Sweatlock, M. T. Sheldon, A. P. Alivisatos, and H. A. Atwater, "Silicon-based plasmonics for on-chip photonics," IEEE Journal of Selected Topics in *Quantum Electronics*, vol. 16, pp. 295-306, 2010.

[89] B. S. Williams, "Terahertz quantum-cascade lasers," *Nature photonics,* vol. 1, p. 517, 2007.

[90] T. Minami, "Transparent conducting oxide semiconductors for transparent electrodes," *Semiconductor science and technology*, vol. 20, p. S35, 2005.

[91] G. J. Exarhos and X.-D. Zhou, "Discovery-based design of transparent conducting oxide films," *Thin solid films,* vol. 515, pp. 7025-7052, 2007.

[92] L. Wang, C. Clavero, K. Yang, E. Radue, M. Simons, I. Novikova, et al., "Bulk and surface plasmon polariton excitation in RuO2 for low-loss plasmonic applications in NIR," *Optics express*, vol. 20, pp. 8618-8628, 2012.

[93] J. Cleary, R. Peale, D. Shelton, G. Boreman, C. Smith, M. Ishigami, et al., "IR permittivities for silicides and doped silicon," JOSA B, vol. 27, pp. 730-734, 2010.

[94] G. V. Naik, J. Kim, and A. Boltasseva, "Oxides and nitrides as alternative plasmonic materials in the optical range," *Optical materials express*, vol. 1, no. 6, pp. 1090-1099, 2011.

[95] M. Wittmer, "Tetragonal nickel oxide films on glass and silicon," J. Vac. Sci. Technol., vol. 3, no. 5, pp. 1797-1799, 1985.

[96] K. S. Novoselov, V. Fal, L. Colombo, P. Gellert, M. Schwab, and K. Kim, "A roadmap for graphene," *Nature*, vol. 490, pp. 192-200, 2012.

[97] G. V. Naik, V. M. Shalaev, and A. Boltasseva, “Alternative plasmonic materials: beyond gold and silver,” *Adv. Mater.*, vol. 25, pp. 3264–3294, 2013.

[98] S. Kassavetis, A. Hodroj, C. Metaxa, S. Logothetidis, J. F. Pierson, and P. Patsalas, "Optical and electronic properties of conductive ternary nitrides with rare- or alkaline-earth elements," *J. Appl. Phys.*, vol. 120, no. 22, p. 225106, 2016.

[99] G. M. Matenoglou, Ch. E. Lekka, L. E. Koutsokeras, G. Karras, C. Kosmidis, G. A. Evangelakis, and P. Patsalas, "Structure and electronic properties of conducting, ternary TixTa1−xN films," *J. Appl. Phys.*, vol. 105, no. 10, p. 103714, 2009.

[100] L. E. Koutsokeras, G. Abadias, Ch. E. Lekka, G. M. Matenoglou, D. F. Anagnostopoulos, G. A. Evangelakis, and P. Patsalas, "Conducting transition metal nitride thin films with tailored cell sizes: the case of δ-TixTa1−xN," *Appl. Phys. Lett.*, vol. 93, no. 1, p. 011904, 2008.

[101] G. M. Matenoglou, L. E. Koutsokeras, P. Patsalas, "Plasma energy and work function of conducting transition metal nitrides for electronic applications," *Appl. Phys. Lett.*, vol. 94, no. 15, p. 152108, 2009.

[102] G. M. Matenoglou, L. E. Koutsokeras, Ch. E. Lekka, G. Abadias, C. Kosmidis, G. A. Evangelakis, and P. Patsalas, "Structure, stability and bonding of ternary transition metal nitrides," *Surf. Coat. Technol.*, vol. 204, no. 6-7, pp. 911-914, 2009.

[103] S. Kassavetis, G. Abadias, G. Vourlias, G. Bantsis, S. Logothetidis, and P. Patsalas, "Optical properties of TixAl1-xN thin films in the whole compositional range," *Surf. Coat. Technol.*, vol. 295, pp. 125-129, 2016.

[104] S. Kassavetis, A. Hodroj, C. Metaxa, S. Logothetidis, J. F. Pierson, and P. Patsalas, "Optical and electronic properties of conductive ternary nitrides with rare- or alkaline-earth elements," *J. Appl. Phys.*, vol. 120, no. 22, p. 225106, 2016.

[105] D. Gall, I. Petrov, and J. E. Greene, "Epitaxial Sc1-xTixN(001): optical and electronic transport properties," *J. Appl. Phys.*, vol. 89, no. 1, pp. 401-409, 2001.

[106] D. Gall, M. Stoehr, and J. E. Greene, "Vibrational modes in epitaxial Sc1−xTixN(001) layers: an ab-initio calculation and Raman spectroscopy study," *Phys. Rev. B: Condens. Matter Mater. Phys.*, vol. 64, no. 17, p. 174302, 2001.

[107] U. Mahajan, M. Dhonde, K. Sahu, P. Ghosh, and P. M. Shirage, "Titanium Nitride (TiN) as a promising alternative to plasmonic metals: A Comprehensive Review of synthesis and applications," *Materials Advances*, Jan. 2024.

[108] A. K. M. Rakib, R. Rahad, Md. O. Faruque, and R. H. Sagor, "ZrN-based plasmonic sensor: a promising alternative to traditional noble metal-based sensors for CMOS-compatible and tunable optical properties," *Optics Express*, vol. 31, no. 15, p. 25280, 2023.

[109] I. Tathfif, K. S. Rashid, A. A. Yaseer, and R. H. Sagor, "Alternative material titanium nitride based refractive index sensor embedded with defects: An emerging solution in sensing arena," *Results in Physics*, vol. 29, p. 104795, 2021.

[110] K. S. Rashid, I. Tathfif, A. A. Yaseer, Md. F. Hassan, and R. H. Sagor, "Cog-shaped refractive index sensor embedded with gold nanorods for temperature sensing of multiple analytes," Optics Express, vol. 29, no. 23, p. 37541, 2021.

[111] K. S. Rashid, Md. F. Hassan, A. A. Yaseer, I. Tathfif, and R. H. Sagor, "Gas-sensing and label-free detection of biomaterials employing multiple rings structured plasmonic nanosensor," Sensing and Bio-sensing Research, vol. 33, p. 100440, 2021.

[112] R. A. Mahmud, Md. O. Faruque, and R. H. Sagor, "Plasmonic Refractive Index Sensor Based on Ring-Type Pentagonal Resonator with High Sensitivity," Plasmonics, vol. 16, no. 3, pp. 873–880, 2021.

[113] S. Sharmin, T. Z. Adry, Md. F. Hassan, E. Surid, and R. H. Sagor, "Numerical investigation of nanodots implanted High-Performance Plasmonic Refractive Index Sensor," Plasmonics, vol. 17, no. 4, pp. 1717–1729, 2022.

[114] A. K. M. Rakib, A. T. B. Siddique, Md. S. Sakib, Md. O. Faruque, and R. H. Sagor, "A numerical analysis of a highly sensitive hexagonal plasmonic refractive index sensor," Optics Communications, vol. 530, p. 129205, 2023.

[115] H. B. Salah, A. Hocini, N. Melouki, and D. Khedrouche, "Design and analysis of near infrared high sensitive metal-insulator-metal plasmonic bio-sensor," IOP Conference Series. Materials Science and Engineering, vol. 1046, no. 1, p. 012003, 2021.

[116] R. Rahad, A. K. M. Rakib, M. A. Haque, S. S. Sharar, and R. H. Sagor, "Plasmonic refractive index sensing in the early diagnosis of diabetes, anemia, and cancer: An exploration of biological biomarkers," Results in Physics, vol. 49, p. 106478, 2023.

[117] I. Tathfif, Md. F. Hassan, K. S. Rashid, A. A. Yaseer, and R. H. Sagor, "A highly sensitive plasmonic refractive index sensor based on concentric triple ring resonator for cancer biomarker and chemical concentration detection," Optics Communications, vol. 519, p. 128429, 2022.